

UNCLASSIFIED

AD NUMBER	
AD126610	
CLASSIFICATION CHANGES	
TO:	UNCLASSIFIED
FROM:	CONFIDENTIAL
LIMITATION CHANGES	
TO: Approved for public release; distribution is unlimited.	
FROM: Distribution authorized to U.S. Gov't. agencies and their contractors; Administrative/Operational Use; SEP 1956. Other requests shall be referred to Army Ballistic Research Lab., Aberdeen Proving Ground, MD.	
AUTHORITY	
30 Sep 1968, DoDD 5200.10; BRL D/A ltr dtd 22 Apr 1981	

THIS PAGE IS UNCLASSIFIED

THIS REPORT HAS BEEN DELIMITED  
AND CLEARED FOR PUBLIC RELEASE  
UNDER DOD DIRECTIVE 5200.20 AND  
NO RESTRICTIONS ARE IMPOSED UPON  
ITS USE AND DISCLOSURE.

**DISTRIBUTION STATEMENT A**

APPROVED FOR PUBLIC RELEASE;  
DISTRIBUTION UNLIMITED.

# UNCLASSIFIED

---

## AD \_\_\_\_\_

*Reproduced  
by the*

ARMED SERVICES TECHNICAL INFORMATION AGENCY  
ARLINGTON HALL STATION  
ARLINGTON 12, VIRGINIA

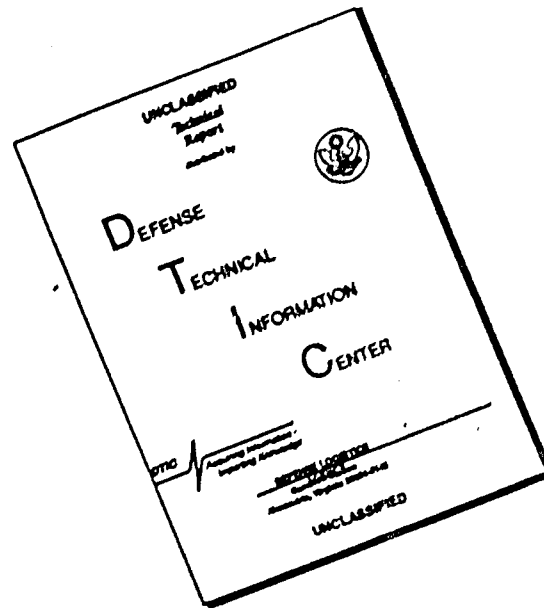


DOWNGRADED AT 3 YEAR INTERVALS:  
DECLASSIFIED AFTER 12 YEARS  
DOD DIR 5200.10

---

# UNCLASSIFIED

# DISCLAIMER NOTICE



THIS DOCUMENT IS BEST QUALITY AVAILABLE. THE COPY FURNISHED TO DTIC CONTAINED A SIGNIFICANT NUMBER OF PAGES WHICH DO NOT REPRODUCE LEGIBLY.

**126610**

**Armed Services Technical Information Agency**

Reproduced by

**DOCUMENT SERVICE CENTER**

**KNOTT BUILDING, DAYTON, 2, OHIO**

RO-CARL

CONTROL ONLY

**1 OF 2**

**NOTICE: WHEN GOVERNMENT OR OTHER DRAWINGS, SPECIFICATIONS OR OTHER DATA IS USED FOR ANY PURPOSE OTHER THAN IN CONNECTION WITH A DEFINITELY RELATED GOVERNMENT PROCUREMENT OPERATION, THE U. S. GOVERNMENT THEREBY INCURS NO RESPONSIBILITY, NOR ANY OBLIGATION WHATSOEVER; AND THE FACT THAT THE GOVERNMENT MAY HAVE FORMULATED, FURNISHED, OR IN ANY WAY SUPPLIED THE DRAWING, SPECIFICATIONS, OR OTHER DATA IS NOT TO BE REGARDED BY ANY PERSON OR CORPORATION, OR CONVEYING ANY RIGHTS OR PERMISSION TO MANUFACTURE, OR SELL A PATENTED INVENTION THAT MAY IN ANY WAY BE RELATED THERETO.**

CONFIDENTIAL

AD No. 26610

ASTIA FILE COPY

**BRL**

000075

REPORT No. 994

SEPTEMBER 1956

**FC**

# The Magnus Characteristics Of A 30-MM Aircraft Bullet (U)

A. S. PLATOU

J. STERNBERG

1957

57 A1

143 11

DEPARTMENT OF THE ARMY PROJECT No. 5B0307002  
ORDNANCE RESEARCH AND DEVELOPMENT PROJECT No. TB3-0426

BALLISTIC RESEARCH LABORATORIES



ABERDEEN PROVING GROUND, MARYLAND

CONFIDENTIAL

**NOTICE: THIS DOCUMENT CONTAINS INFORMATION AFFECTING THE  
NATIONAL DEFENSE OF THE UNITED STATES WITHIN THE MEANING  
OF THE ESPIONAGE LAWS, TITLE 18, U.S.C., SECTIONS 793 and 794.  
THE TRANSMISSION OR THE REVELATION OF ITS CONTENTS IN  
ANY MANNER TO AN UNAUTHORIZED PERSON IS PROHIBITED BY LAW.**

**CONFIDENTIAL**

BALLISTIC RESEARCH LABORATORIES

REPORT NO. 994

SEPTEMBER 1956

THE MAGNUS CHARACTERISTICS OF A 30 MM AIRCRAFT BULLET (U)

A. S. Platou

J. Sternberg

Department of the Army Project No. 5B0307002  
Ordnance Research and Development Project No. TB3-0426

ABERDEEN PROVING GROUND, MARYLAND

57AA  
**CONFIDENTIAL**

14311



# CONFIDENTIAL

## TABLE OF CONTENTS

	PAGE
ABSTRACT. . . . .	5
SUMMARY . . . . .	7
TABLE OF SYMBOLS. . . . .	8
I. INTRODUCTION. . . . .	11
II. EXPERIMENTAL PROCEDURE. . . . .	12
A. THE MODEL AND INSTRUMENTATION . . . . .	12
B. MODEL SUPPORT AND TUNNEL INTERFERENCE . . . . .	15
C. REDUCTION OF TEST DATA. . . . .	18
III. RESULTS . . . . .	20
IV. COMPARISON WITH THEORY. . . . .	22
V. FREE FLIGHT COMPARISON. . . . .	24
VI. CONCLUSIONS . . . . .	25
VII. REFERENCES. . . . .	26
VIII. FIGURES. . . . .	27
A. CONFIGURATION DIMENSIONS AND FLIGHT CHARACTERISTICS . . . . .	28
B. INSTRUMENTATION AND SUPPORT INTERFERENCE DATA. . . . .	32
C. NORMAL FORCE VS. SPIN . . . . .	45
D. THE MODEL BOUNDARY LAYER. . . . .	48
E. THE MAGNUS DATA . . . . .	50
APPENDIX I. . . . .	57
DISTRIBUTION. . . . .	63

## **CONFIDENTIAL**

### **ACKNOWLEDGMENT**

The authors wish to acknowledge the important contributions of other members of the wind tunnel group in carrying out this program. We particularly wish to mention the aid received from the Instrumentation Section, headed by Dr. T. L. Smith, in developing the air turbine, the strain gage balance, and the model balancing technique, and the assistance of Mr. E. Bluestone in solving the model design problems.

**CONFIDENTIAL**

BALLISTIC RESEARCH LABORATORIES

REPORT NO. 994

ASPlatou/JSternberg/rf  
Aberdeen Proving Ground, Md.  
September 1956

THE MAGNUS CHARACTERISTICS OF A 30 MM AIRCRAFT BULLET (J)

ABSTRACT

Magnus and pitch plane data at  $M_\infty = 1.5$  to  $2.5$  have been obtained on a small fineness ratio ( $l/d = 3$ ) body of revolution. Data have been obtained at angles of attack up to  $40^\circ$  under turbulent boundary layer conditions. The Magnus data are non-linear with spin and with angle of attack and the Magnus force at most spin conditions is negative in the low angle of attack region.

**CONFIDENTIAL**

# CONFIDENTIAL

## SUMMARY

Magnus force and pitching moment data have been obtained on a model of a 30mm aircraft bullet in the Mach number range of 1.5 to 2.5. These data cover angles of attack up to  $40^\circ$  and spin rates up to 45,000 RPM which include the spin rates of the prototype. The Magnus force and moment are non-linear with spin and with angle of attack and are negative in the low angle of attack range. The Magnus center of pressure is located on the rear portion of the configuration for all of the conditions where it could be accurately measured. The normal force and pitching moment are only very slightly dependent on spin.

# CONFIDENTIAL

## TABLE OF SYMBOLS

### Air Characteristics

- $a$  = speed of sound
- $U_g$  = Bullet muzzle velocity with respect to gun
- $U_a$  = Bullet velocity with respect to air
- $U_{ts}$  = Test section velocity
- $P_o$  = Stagnation pressure
- $P_{ts}$  = Test section static pressure
- $T_o$  = Stagnation temperature
- $q$  = Dynamic pressure =  $\frac{1}{2} \rho U_{ts}^2$
- $\rho$  = Density of air
- $\mu$  = Viscosity of air
- $Ma$  = Mach number
- $Re$  = Reynolds No. =  $\frac{\rho u d}{\mu}$

### Model and Balance Dimensions and Constants

- $D$  = Prototype body diameter
- $d$  = Model body diameter
- C.G. = Center of gravity = 1.32 cal. from the base

### Angles

- $\alpha$  = Angle of attack
- $\Gamma$  = Gun traverse angle
- $\omega$  = Bullet spin rate rad./sec (plus is clockwise looking upstream)
- $v_g = \frac{\omega d}{U_g}$  = non-dimensional spin rad/cal. (with respect to gun)
- $v_a = \frac{\omega d}{U_a}$  = non-dimensional spin rad/cal. (with respect to air)

# CONFIDENTIAL

## TABLE OF SYMBOLS (Cont'd)

### Forces and Moments

$$k_N = \frac{N}{\rho U_{ts}^2 d^2} = \text{Normal force coefficient}$$

$$k_m = \frac{m}{\rho U_{ts}^2 d^3} = \text{Pitching moment coefficient (about C.G.)}$$

$$k_F = \frac{F}{\rho U_{ts}^2 d^2 \left( \frac{\omega d}{U_{ts}} \right)} = \text{Magnus force coefficient (plus is to left looking upstream)}$$

$$k_T = \frac{T}{\rho U_{ts}^2 d^3 \left( \frac{\omega d}{U_{ts}} \right)} = \text{Magnus moment coefficient (about C.G.) (plus is plus force ahead of the C.G.)}$$

$$K_T = \frac{T}{\rho U_{ts}^2 d^3 \left( \frac{\omega d}{U_{ts}} \right) \sin \alpha} = \text{Ballistics Magnus moment coefficient } (\alpha \text{ in radians})$$

$$K_T = \frac{dk_T}{d\alpha} \text{ at small } \alpha$$

# CONFIDENTIAL

## INTRODUCTION

The use of spin stabilized bullets for the tail defense of very high speed bombers introduces new problems in the prediction of the bullet trajectories. In general, the bullet is to be launched from the gun at some angle to the flight path of the plane, and since the speed of the plane and the muzzle velocity of the gun are comparable, the bullet may start its flight at large angles of yaw. For a typical bullet shown in Fig. 3, initial yaw angles over  $40^\circ$  may be attained; further the subsequent motion may result in even higher yaw angles near the gun muzzle. To aid in predicting the bullet trajectories at these angles of attack a considerable amount of aerodynamic information for the bullet must be obtained.

It is well known that spin affects the aerodynamic forces on a body of revolution. Besides possible effects on the normal and drag forces the spin can generate an entirely new force, called the Magnus force, which acts in a direction perpendicular to the axis of the body and perpendicular to the angle of attack plane. It is also known that at small angles of attack the Magnus moment is often of great importance in determining the dynamic stability of projectiles and it seems reasonable to expect the Magnus moment to be also of importance at large angles of attack. In order to obtain knowledge of the Magnus forces at both large and small angles of attack, the instrumentation and test procedure described in this report have been developed.

We have been able to cover only a portion of the angle of attack - Mach number range shown in Fig. 1. At the lower supersonic Mach numbers the tunnel walls interfere with the flow about the model especially at the larger angles of attack, so we limited the tests to Mach numbers of 1.57, 2.0, and 2.47. Tests could have been performed at lower supersonic Mach numbers if we had a reduced model diameter. However, since the bullet is only 3 calibers long, a model diameter significantly less than the diameter chosen (2") would have forced us to place the strain gage balance downstream of the model, thereby reducing the accuracy of the

## CONFIDENTIAL

measurements. The circled points in Fig. 1 indicate the maximum angle of attack conditions at which reliable data have been obtained. Fig. 2 indicates the test Reynolds numbers compared to the free flight Reynolds numbers.

The wind tunnel model must produce the same non-dimensional spin (rad/cal. of forward travel) as the prototype in free flight. Since the prototype always leaves the gun with the same spin ( $v_g$ ), the initial non-dimensional spin ( $v_a$ ) is only dependent on the resultant velocity of the bullet, hence

$$v_a = \frac{\omega D}{U_a} = v_g \frac{U_g}{U_a}$$

Fig. 1 shows the values of  $v_a$  which are required for the 30mm bullet for which  $v_g = .28$ . The model spin rates (rad./sec) are

$$\omega = v_a \frac{U_{ts}}{d}$$

This corresponds to spin rates up to 45,000 RPM for the 2 inch diameter model tested at Mach No. 1.57. At Mach No. 2.47 the same model must spin at 36,000 RPM.

## II EXPERIMENTAL PROCEDURE

### A. The Model and Instrumentation

The two inch diameter model of the 30mm aircraft bullet is shown in Fig. 3. All external dimensions are proportionately scaled from the prototype except for the grooves in the rotating band. The model grooves are of the proper width, depth, and cant, however the "slurring over", Fig. 4, which is created on one side of the groove as the prototype moves in the gun barrel, is not duplicated. The "slurring over" would be difficult to duplicate and its effect on the Magnus data is probably small compared to the effect of the grooves themselves.



## CONFIDENTIAL

The air motor is an integral part of the model, the model forming the outside surface of the revolving portion of the motor. This portion of the motor is mounted on the bearing outer races as shown in Fig. 5. The inner races of the bearing are mounted on a cylinder which in turn is mounted on the upstream end of the model strain gage balance and supporting strut. The model is rotated by an impulse air turbine with the turbine buckets being mounted in the model base and the air nozzles, of which there are four, being mounted just upstream of the buckets on the supporting strut. An axial hole drilled in the supporting strut serves as a passage for the high pressure air to the nozzles; at the usual test conditions the flow out of the nozzles should be approximately Mach number 4. Since the nozzle air is exhausted into the tunnel, dry air from the wind tunnel storage sphere is used as the high pressure source.

For these tests sufficient power to operate the motor easily was obtained by using a supply pressure of 175 psi. Under the test conditions the motor has a starting torque of 1.2 in. lbs. and develops .5 HP at 45,000 RPM. The acceleration time from 0 to 45,000 RPM is approximately 30 sec.

A spring is used to preload the bearings so that the bearings are subjected to a thrust at all times. The preload appears to confine the ball rotation to one axis, because a track is worn into the ball surface after several thousand revolutions, Fig. 6. A thermocouple is mounted near the forward end of the strut so that the temperature rise of the strut can be measured when the model is spun. While breaking in a set of bearings, the appearance of a well worn track is indicated by a leveling off or decrease in the temperature of the forward end of the strut. After several minutes of running at low speeds the temperature stops rising and may in the case of an extremely good bearing start decreasing. Bearings are broken in by measuring the strut temperature at 10,000 and 20,000 RPM and no bearings are run at higher speeds until no temperature increase is obtained at the low speeds. If the preload is

## CONFIDENTIAL

removed from the bearing, the bearing balls will reorient themselves and a rebreaking in one of the bearings is necessary.

Measurement of the temperature of the forward end of the strut is also necessary during the tunnel tests for it indicates the condition of the bearings during any one spin period. If the temperature rise becomes excessive or if the temperature of the strut rises above 150° F the bearings are rinsed in a clear solvent and regreased. The 150 degree F limit was found to be just under the temperature at which freezing of the bearings might occur.

Two permanent magnets are mounted near the base of the model (see Fig. 5). As the model rotates, the magnetic field generates a current in a coil mounted on the stationary strut. Using suitable circuitry, the resultant coil signal is converted into a signal proportional to the RPM of the model.

Dynamic balancing of the model is accomplished using a sensitive balancing rig which determines the location and amount of metal to be removed from both the nose and tail of the model. The balancing reduces the wear on the bearings especially at resonant speeds and reduces the strain gage signal oscillations at resonant speeds. Necessarily, readings are not taken near the resonant points.

In practice, the strain gage hinge lines were not positioned exactly as desired. The angles and lengths, which are needed to sort out the pitching and yawing moments, are measured by means of a static calibration described in Appendix I. The desired moments could then be determined by solving a set of four simultaneous equations. As will be noted later, however it was possible to considerably simplify the reduction procedure.

Temperature compensation of the strain gage bridges was accomplished by varying the resistance of one of the bridge legs until the bridge indicated no unbalance when the temperature of the beam was

## CONFIDENTIAL

changed. During test, temperature non-uniformity of the beam caused by heat from the bearings might still cause trouble, so as a check, the bridge unbalance was observed as the model spin varied from 45,000 RPM to 0 under no flow conditions. No bridge unbalance was found, except at resonant speeds, so the method of temperature compensation was considered satisfactory.

The model was tested on two different support systems. The power lead lengths for each of these installations differed, and it was necessary to correct the bridge sensitivity for the differences in the power lead resistances.

### B. Model Support and Tunnel Interference

Comparisons of wind tunnel base pressures with free flight base pressures on the same model at the same test conditions have shown that if the wind tunnel support system is made small enough, the tunnel and free flight measurements are in reasonable agreement. However, in most cases, the model loads are too large to allow the use of a support system which does not change the wake flow. On a cylindrical body at small angles of attack, with a convergent wake, the change in the upstream flow is of negligible importance. If the support system interference is large enough to diverge the wake flow the resultant shock wave at the model base may cause separation of the boundary layer on the model surface. It would then be possible for the support system to affect the flow over an extensive region of the body. If this separation does not occur, then measurements of the model forces, with the exception of the base force should be valid.

As long as the flow relative to the model surface is supersonic, the Magnus force and moment measurements should be free of support interference. When the flow is supersonic relative to the model, shock waves arising from the irregularities of the model surface near the base, are clearly visible in the Schlieren photographs. Fig. 7 shows the model at an angle of attack where the flow is everywhere supersonic. In Fig. 8

## CONFIDENTIAL

the flow separates on the top side of the model near the nose and there is a very extensive subsonic wake. As will be described below the photographic observations were supplemented with normal force and pitching moment measurements on a non-rotating model. As could be expected, the development of an extensive wake caused large changes in the model forces.

A limited series of measurements were made at  $Ma = 2.0$ ,  $\alpha = 10^\circ$ , and  $20^\circ$  to confirm the supposition that the Magnus forces would be independent of the wake flow. The wake flow was altered by placing rings on the strut just aft of the model base and no changes in the Magnus force were found.

The tests of the various support configurations were made by measuring the normal force and pitching moment on a non-spinning model. Magnus force measurements on a spinning model with a series of different struts would have been very time-consuming and expensive; however, it was possible that the non-spinning tests might not be satisfactory. The model spin alters the boundary layer on the model in a complicated way, and it is possible that the altered boundary layer might be more susceptible to separation than the boundary layer on the non-spinning model. However, in the latter case, the normal force or pitching moment should have been significantly affected by the model spin; all of the test data indicated a negligible influence of spin on the pitch plane forces.

At large yaw angles, the direction of the wake axis is intermediate between the strut axis and the free stream flow direction. We thought that the strut interference might be minimized if the strut axis coincided with the wake axis, because then the initial portion of the strut would be in a low speed flow and the pressure changes produced by the strut would be relatively small. Fig. 9 shows the strut arrangement that was used to vary the angle between the strut axis and the model axis. Fig. 10 shows how these different struts were connected to the tunnel angle of attack system to allow testing of the model in a given angle of attack range with a series of different struts. The Schlieren pictures suggest that the development of a subsonic region on the model

## CONFIDENTIAL

was largely determined by flow interference from portions of the model support system other than the strut at the model base. In particular, interference from the downstream portion of the strut and the piece connecting the strut to the angle of attack system probably had as much or more to do with the resultant flow as the angle between the strut and model axis. The four Schlieren photographs (Fig. 11) at  $\alpha = 40^\circ$ ,  $M = 1.57$ , as well as the peculiar rise in the pitching moment curve near that angle of attack, (see Fig. 13) indicate the development of large wakes although the degree of separation differed for the different struts. With the  $B = 0^\circ$  strut, there was a reflected shock from the Mach intersection near the wall, which intersected the wake a little over one model diameter from the base. With the  $B = 30^\circ$  strut, the reflected shock struck the wake much further downstream and the degree of separation appeared to be much reduced. Fig. 12 shows the same four strut configurations at  $\alpha = 30^\circ$  at  $M = 1.57$ . At this angle of attack both the Schlieren photographs and the pitch plane data indicated interference free results. As at  $\alpha = 40^\circ$ , the reflected shock system for  $B = 0^\circ$  strut intersected the wake closer to the model base than the reflected shock for the other struts; however the reflected shock was still  $2\frac{1}{2}$  model diameters from the base.

At  $M = 1.57$  and  $M = 2.0$ , we felt there was little to choose between the several strut configurations. The presumptive evidence indicates that there was some interference present for all of the configurations above  $\alpha = 32^\circ$  at  $M = 1.57$ , and  $\alpha = 44^\circ$  at  $M = 2.0$ . At  $M = 2.47$ , the maximum  $\alpha$  required was only  $20^\circ$  so that strut interference was not a problem. In view of these results, a coaxial strut was used for all of the measurements.

While the main objective of these tests was to obtain Magnus data at large yaw, we had a strong interest in obtaining accurate data at small yaw. Unfortunately, the precision we desired at small yaw could not be achieved using the tunnel angle of attack system. The support system deflects easily in the horizontal plane and further, the

## CONFIDENTIAL

attachment of the strut support to the guiding crescent is imperfect, and a small amount of inelastic movement is possible. Careful measurements showed that the uncertainty in yaw angle due to the existing side-play was not particularly important. However, when tested the model oscillated a small amount in the horizontal plane with an irregularly varying amplitude. The resultant oscillation of the yawing moments greatly reduced the accuracy of the measurements. To provide a more rigid support for the model, a door mount (see Fig. 16) was used at all of the Mach numbers. (See Figs. 13-15). It was still necessary, however, to make some experiments at small yaw with the tunnel angle of attack system. The door mount does not have a window for Schlieren observation and flow observations were needed to clarify some of the initial results.

Normal force and pitching moment measurements obtained using the door mount are also shown in Figs. 13-15. Flow interference appears to occur at  $\alpha = 25^\circ$  at  $M = 1.57$  and at  $\alpha = 34^\circ$  at  $M = 2.00$ . The angle of attack on the door mount was changed by externally rotating a disk; the swept back double wedge support holding the model strut was connected to the disk. As the model angle of attack was increased, the angle of attack of the support also increased. Further, it simultaneously moved close to the floor of the tunnel. We believe that the resultant strong shock system caused flow separation on the model. A special model strut has now been fabricated which is bent  $22^\circ$  at the model base. With this new strut the support system flow disturbances should be greatly reduced and it should be possible to use the door mount over the entire angle of attack range, if desired. Actually at large yaw, since the measured forces are larger, the scatter introduced by the oscillations of the model mounted on the tunnel angle of attack system are not important.

### C. Reduction of Test Data

Because of imperfections in the tunnel flow and imperfect alignment and/or tracking of the angle of attack systems that were used, the resultant angle of attack of the model with respect to the airstream is, in general, not in a vertical plane through the tunnel axis. Therefore, the



## CONFIDENTIAL

yawing moment at no spin will not be zero and will vary with the model angle of attack. In addition, there will be an apparent yawing moment because the yawing moment hinge lines are not parallel and in the plane of the angle of attack. During installation of the model in the tunnel an adjustment of the balance roll angle is made to limit, as far as is practicable, these no spin yawing moments.

The deflection of the model support system under load introduced some possible additional complications in obtaining the Magnus forces. For instance, if the pitch plane forces changed substantially with spin, the angle of attack might vary significantly with spin. Fortunately, as was noted previously, the pitch plane forces were practically invariant with spin (Fig. 17-19). Similarly, the Magnus forces themselves will deflect the support system in the horizontal plane thereby changing the direction of the resultant angle of attack. Hence there will be yawing moments due to the inclination of the normal force vector which have to be subtracted from the total yawing moments to obtain the Magnus moments themselves.

Strut deflection constants were obtained for vertical and horizontal loads. The pitch plane constants were used to correct the vertical component of the angle of attack and the lateral constants were used to determine the yawing moment due to the inclination of the normal force vector. The Magnus force in these tests was always small so that the change in the lateral component of the angle of attack caused by the Magnus force was always small (.01 degrees was the maximum deflection computed). Hence the apparent Magnus force due to the inclination of the normal force vector can be shown to be

$$\Delta N = N \frac{\sin \Delta \theta}{\tan \alpha}$$

where  $\Delta \theta$  is the change in the lateral component of  $\alpha$ .

The resulting error in the Magnus force is within the experimental accuracy and therefore was not included in the reduction.

## CONFIDENTIAL

The normal force contribution to the measured yawing moment was computed in several critical cases and was found to be negligible. As a result, it was possible to determine the Magnus data by simply subtracting the yawing moment at zero spin for each angle of attack.

### III. RESULTS

The first experiments were made at  $M = 2.0$  at small angles of attack and very curious results were obtained. The Magnus moments could be repeated consistently at various spin rates, but the zero spin yawing moment was different almost every time the model stopped. The spread in the zero spin yawing moment values was too large to disregard when compared with yawing moment variations observed with changes in spin rate. Also the Magnus force varied non-linearly with spin and extrapolation of the data to zero spin appeared hazardous. It was soon found that the yawing moment was a single valued function of the roll angle at which the model happened to stop during each test. Shadowgraphs of the model (see Fig. 20) at different roll angles suggested that the boundary layer transition on the model surface was largely controlled by small imperfections of the model surface, since the position of transition on the top and bottom elements, as shown in the photographs, was different for different roll angles. Even if the model were perfectly made and at zero angle of attack, it would be unlikely that the transition would occur at the same axial position all around the model because of the influence of non-uniformities in the tunnel flow. But in the latter case, the transition pattern would have remained fixed with respect to the tunnel coordinates and so would not have been troublesome. A difference in the axial position of the boundary layer transition around the model implied a difference in boundary layer displacement thickness at downstream axial stations. The "effective" body would then not be at zero lift, and there would be some pitching and yawing moment on the model. Such yawing moments on this model are probably larger than those that would be found on a smoothly contoured model because of the presence of the rotating band. Fig. 20 shows that when the boundary layer is laminar ahead of the rotating band that boundary layer separation occurs well upstream of the rotating band.



## CONFIDENTIAL

It is not possible to calculate with any reliability from the photographs what changes in moment should have been produced, since the data are necessarily incomplete. Estimates indicate that small changes in the effective angle of attack of the order of  $.02^\circ$  -  $.03^\circ$  would have been sufficient to account for the measurements. At any reasonable spin rate, any force dependence on roll angle would be averaged by the instrumentation. As the angle of attack is increased, the effect of the angle of attack on transition on the body becomes more and more important. Above about  $7^\circ$ , the dependence of the transition on the model roll angle becomes negligible. When the Reynolds number was increased from  $.62$  to  $.94 \times 10^6$ , the transition occurred fairly well forward on the body (Fig. 21). The resultant yawing moment variation, which was about half the variation experienced at the lower Reynolds number was about the same magnitude as the uncertainty in reading the data, and was considered to be acceptable. Similar results were achieved at the lower Reynolds number by using a boundary layer trip ring near the base of the ogive.

The data obtained at the higher Reynolds numbers at three Mach numbers, 1.57, 2.00, and 2.47, are shown in Figs. 22-24. The maximum value of the spin parameter  $\frac{\omega d}{U}$  was approximately the same as the  $\frac{\omega d}{U}$  values for the shell when it has the air Mach numbers shown, at launching. It is seen that the Magnus force reverses direction at small angles of attack. These low angle of attack tests were rerun several times to confirm that the reversal was definitely present. Furthermore, it is clear that at small angles of attack the Magnus forces and moment vary non-linearly with spin. Although the data above  $10-15^\circ$  are not shown, in Figs. 22-24, the Magnus force and moment are reasonably linear with spin and can be obtained from Figs. 25-27.

Figures 25-27 are cross plots of the data at the free flight values of the non-dimensional spin parameter. As would be expected from Figs. 22-24, the Magnus force is also non-linear with yaw. The data at all three Mach numbers indicate that the center of the pressure of the Magnus forces changes

## CONFIDENTIAL

with angle of attack and that the Magnus force coefficient reaches a peak value at about  $15 - 20^\circ \alpha$ . At angles of attack below  $5^\circ$ , the accuracy of the center of pressure determination is poor and so it has not been entered on the graphs. The data at  $M = 1.57$  and  $2.00$  also indicate that the Magnus force coefficient approaches a constant value at about  $30^\circ \alpha$ . Certainly it is not safe to extrapolate these data to still larger angles of attack.

### IV. COMPARISON WITH THEORY

As far as we know, no adequate theory exists at the present time for predicting the Magnus forces on the model used in these tests. The principal theoretical work that has been done has been directed towards calculating the Magnus forces at small angles of attack, with laminar boundary layers, on very simple body shapes. It is found that the boundary layer on the model is altered by the combined effects of angle of attack and spin. The resulting displacement thickness distribution is not symmetrical with respect to the vertical plane, so that Magnus forces can be produced. Also there may be a significant force contribution arising from asymmetry of the skin friction forces. The existing solutions <sup>1,2</sup> assume an incompressible flow and do not account for the actual boundary layer development on the nose. In addition, because of the disturbance produced by the rotating band, at Mach numbers of  $1.57$  to  $2.47$ , we were not able to test with a laminar boundary layer over the whole model length at any angles of attack.

Figures 22-27 show that at angles of attack less than  $5^\circ$ , the Magnus force is negative, opposite in sign to the small angle force predicted for the laminar boundary layer case. The large B.R.L. free flight range has also obtained indications of negative Magnus forces (see free flight comparison section) on this configuration. However, measurements at the Naval Ordnance Laboratory on bodies with greater length to diameter ratios (about 7) do not show negative Magnus forces. This may be caused by different boundary layer conditions or by the larger fineness ratio. As yet we have been unable to determine the cause of this behavior.

## CONFIDENTIAL

The source of the Magnus forces at large angles of attack is probably entirely different. The normal forces on non-rotating bodies are reasonably well described using the ideas of H. J. Allen<sup>3</sup> with further refinements by Kelly<sup>4</sup>. If we apply these ideas to the prediction of the Magnus force at large angles of attack, we have to relate the Magnus force on a given section of the body to the Magnus force on a spinning cylinder oriented normal to the flow. The "normal" velocity for each section is taken to be the component of the free stream velocity normal to the body axis. Further, the Magnus forces on the sections have to be related, not to the steady state Magnus forces on a cylinder, but rather to the force on a rotating cylinder, impulsively started from rest, before it has developed the steady state force. The forces on forward body sections correspond to short travel distances for the cylinder, the rearward body sections to relatively large travel distances for the cylinder. At any angle of attack, the steady state forces may finally be reached on the body if the body is long enough. Unfortunately, the required low speed starting data are not available.

Further, the whole picture should change at large free stream Mach numbers and angles of attack because the Mach number component normal to the axis will approach and may exceed unity. The development of Magnus forces on a cylinder normal to the flow should be markedly dependent on the flow Mach number. At low speeds, the cylinder rotation causes the point of boundary layer separation to differ on the top and bottom of the cylinder. As a result, the vorticity of opposite sign shed at the top and bottom is not equal and there is a net amount of vorticity of one sign shed in the cylinder wake. As this happens, a circulation of the opposite sign develops around the cylinder and the pressure distribution over the whole cylinder is altered resulting in a Magnus force. When the flow is supersonic, unequal vortex shedding in the wake has a much more restricted field of influence, since its effect is restricted to the subsonic portion of the flow field, except in so

## CONFIDENTIAL

far as it may alter the points of separation of the boundary layers. The Magnus force that results is then due to a change of pressure over a small portion of the cylinder. Furthermore, at low speeds, a relatively large amount of time is required to establish the steady state force since time must be allowed for the development of the starting vortex and then its subsequent movement downstream. At supersonic speeds, the rate of approach to steady state values will depend on the relative importance of the spin and the wake conditions in determining the separation points on the cylinder. If the spin is dominant, then a steady state pressure distribution on the cylinder would be reached very rapidly.

Further, most of the experiments that have been performed on rotating cylinders have either been at very low Reynolds numbers or in the transition region. Data for a turbulent boundary layer would be more appropriate for the type of model used in these tests.

### V. FREE FLIGHT COMPARISON

This same 30mm shell has been fired in the ERL Free Flight Aerodynamics Range. The normal range reduction technique, which is based on the assumption that the forces and moments are linear with spin and angle of attack, would be clearly unsatisfactory in this case. Recently C. H. Murphy<sup>6</sup> has developed a method for deducing the aerodynamic coefficients from a free flight firing when the coefficients are non-linear with angle of attack. In its simpler form, the method requires a cubic or quintic fit to the actual Magnus moment curve. In spite of the fact that the experimental curve cannot be readily approximated in this way, Murphy has analysed the range results and has obtained a Magnus moment curve which is qualitatively similar to the wind tunnel curve. The Magnus moment reverses sign at about the same angle of attack and also reaches a maximum at a moderately large angle of attack.

## CONFIDENTIAL

### VI. CONCLUSIONS

The following conclusions can be drawn from these data:

1. The normal force and pitching moment are only slightly dependent on spin.
2. The Magnus force is non-linear with angle of attack, and at all except the very high spin rates the force and moment change sign at the low angles of attack.
3. The Magnus force and moment do not become linear with spin until an angle of attack between  $7\frac{1}{2}^{\circ}$  and  $15^{\circ}$  is reached. The angle of attack for linearity decreases as the Mach number increases.
4. The Magnus force center of pressure is located behind the center of gravity.
5. The Magnus force and moment decrease as the Mach number increases.
6. The Magnus force and moment are negative at small angles of attack and moderate spin rates. For these data, boundary layer transition occurred before the base of the ogive.
7. A maximum in Magnus force and moment was reached between  $15-20^{\circ}\alpha$  and the Magnus forces varied little with  $\alpha$  near  $\alpha = 30^{\circ}$ . In this larger angle of attack range, the results appeared to be independent of Reynolds number changes produced by changing the tunnel pressure level by a factor of 2.

*A. S. Platou*

A. S. PLATOU

*J. Sternberg*

J. STERNBERG

# CONFIDENTIAL

## VII. REFERENCES

1. Martin, J. C. - "On Magnus Effects Caused by Boundary Layer Displacement Thickness on Bodies of Revolution at Small Angles of Attack". BRL Report 870.
2. Kelly, H. R. - "An Analytical Method for the Magnus Forces and Moments on Spinning Projectiles". NOTS T.M. 1634
3. Allen, H. J., Perkins, E.W. - "A Study of the Effects of Viscosity on Flow over Slender Bodies of Revolution". NACA Rep. 1948.
4. Kelly, H. R. - "The Estimation of Normal Force and Pitching Moment Coefficients for Blunt-Based Bodies of Revolution at Large Angles of Attack". NOTS T.M. 998
5. Luchuk, W., Sparks, W. - "Wind Tunnel Magnus Characteristics of the 7 Cal. A.N. Spinner Rocket". NAVORD Rept. 3813
6. Murphy, C. H. - "The Measurement of Non-Linear Forces and Moments by Means of Free Flight Tests". BRL Rept. 974.

# CONFIDENTIAL

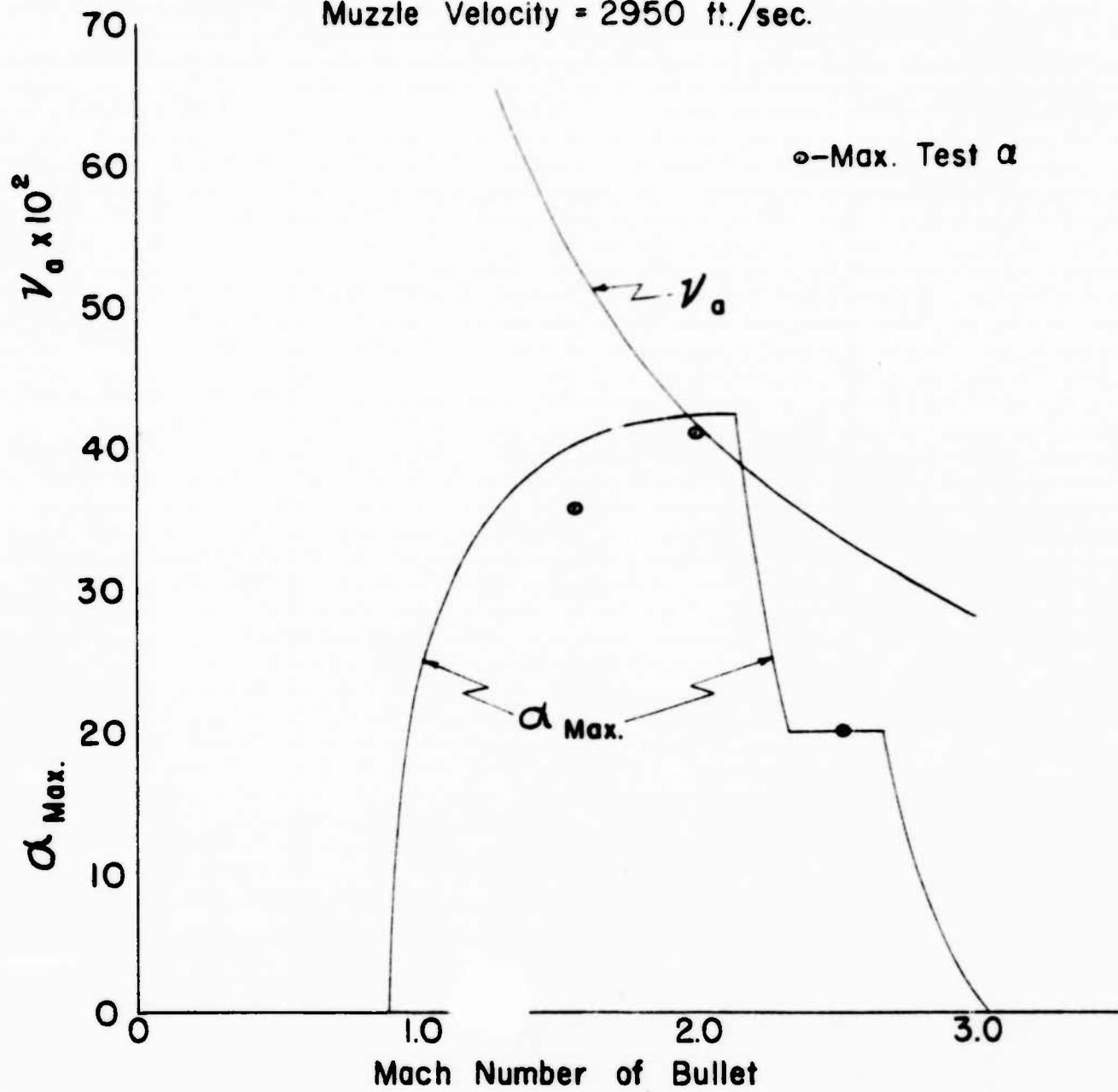
## VIII. FIGURES

- |  |                  |
|--|------------------|
| A. Configuration Dimensions and Flight Characteristics | - Figs. 1 to 4   |
| B. Instrumentation and Support Interference Data       | - Figs. 5 to 16  |
| C. Normal Force vs. Spin                               | - Figs. 17 to 19 |
| D. The Boundary Layer                                  | - Figs. 20 to 21 |
| E. The Magnus Data                                     | - Figs. 22 to 27 |

CONFIDENTIAL

Maximum Aircraft Velocity = 2000 ft./sec.

Muzzle Velocity = 2950 ft./sec.



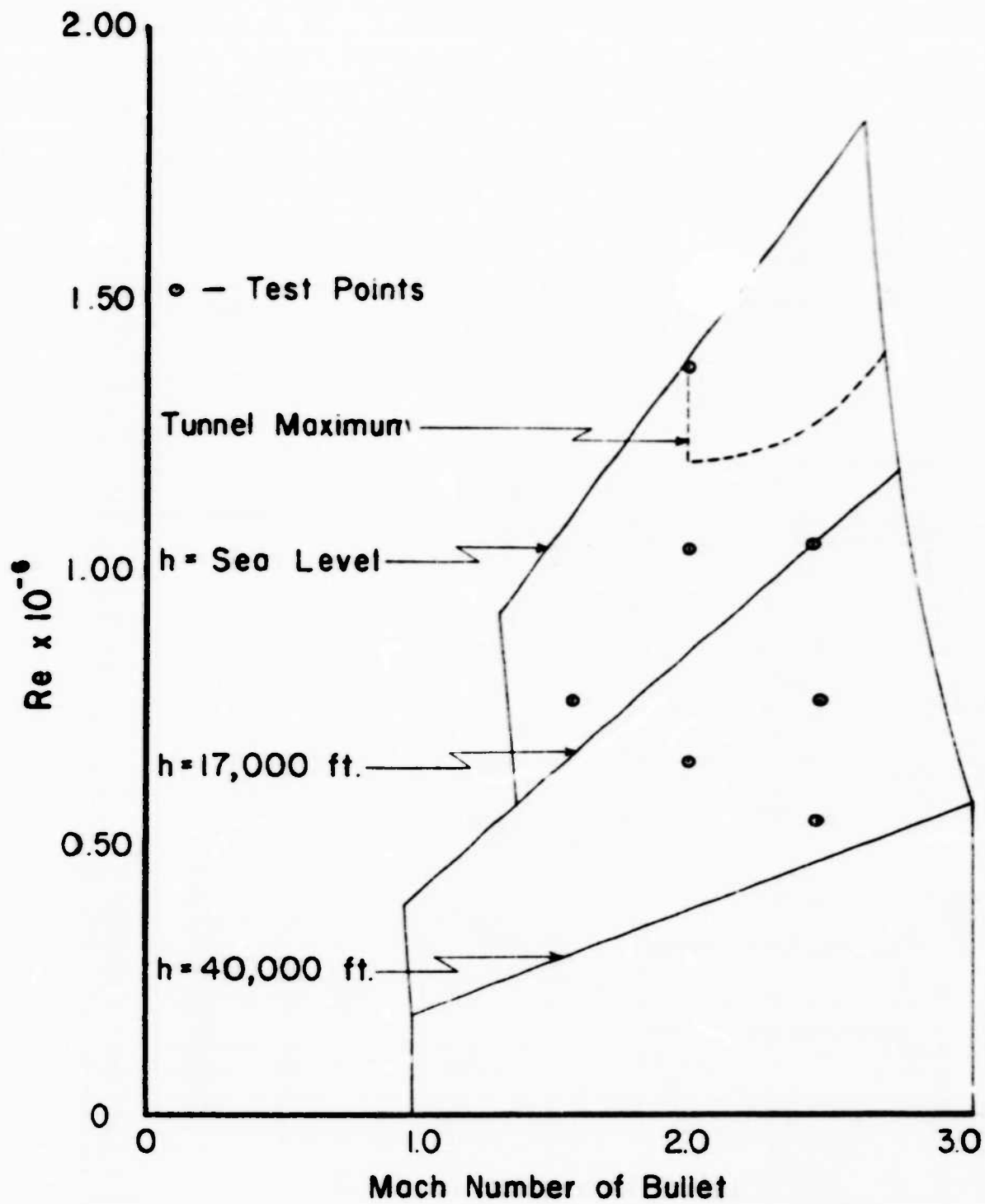
FLIGHT CONDITIONS FOR 30 MM AIRCRAFT BULLET

FIG. 1

CONFIDENTIAL



CONFIDENTIAL

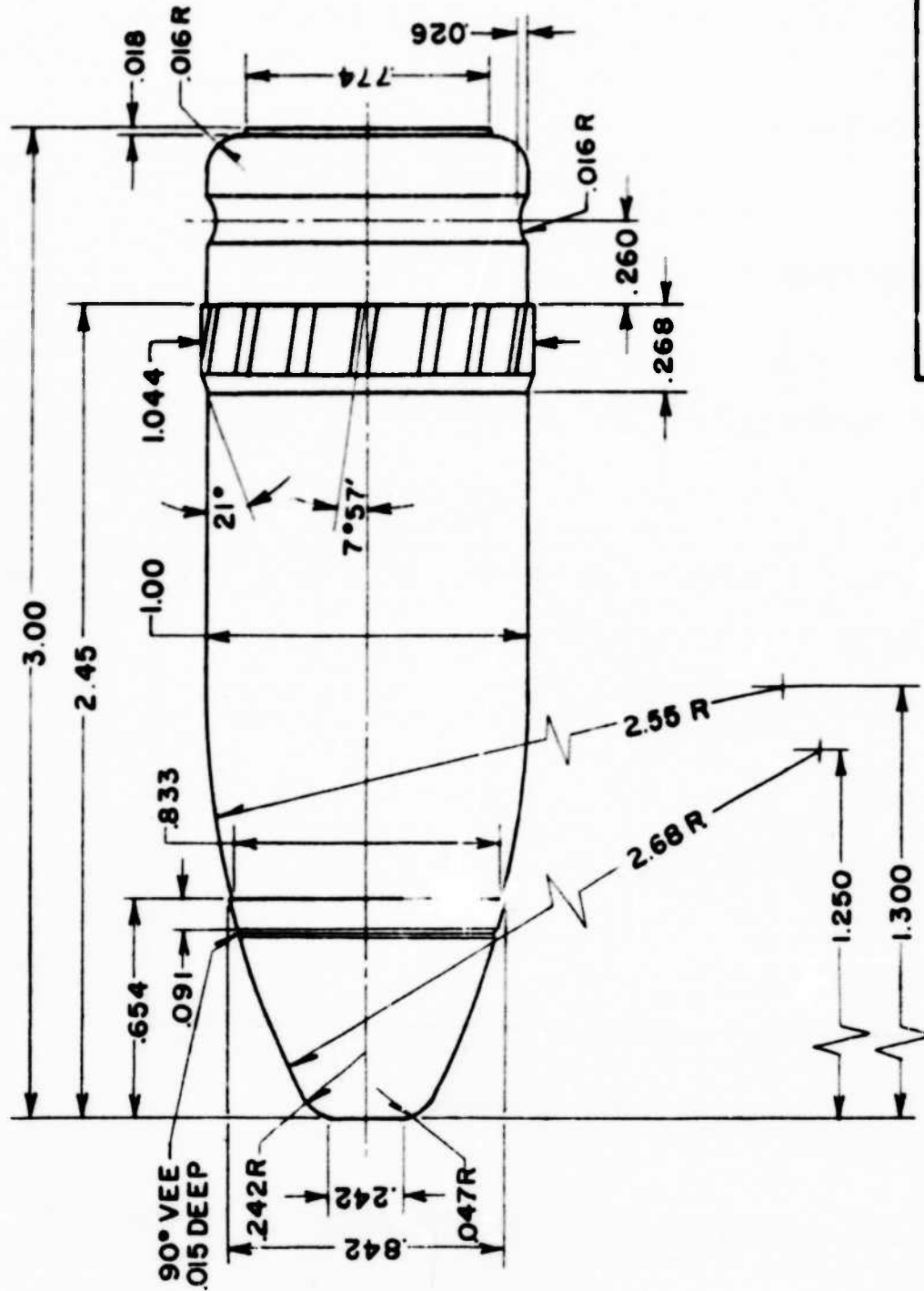


FLIGHT REYNOLDS' NUMBER FOR 30 MM AIRCRAFT BULLET

FIG. 2

CONFIDENTIAL

CONFIDENTIAL



30 m/m BULLET

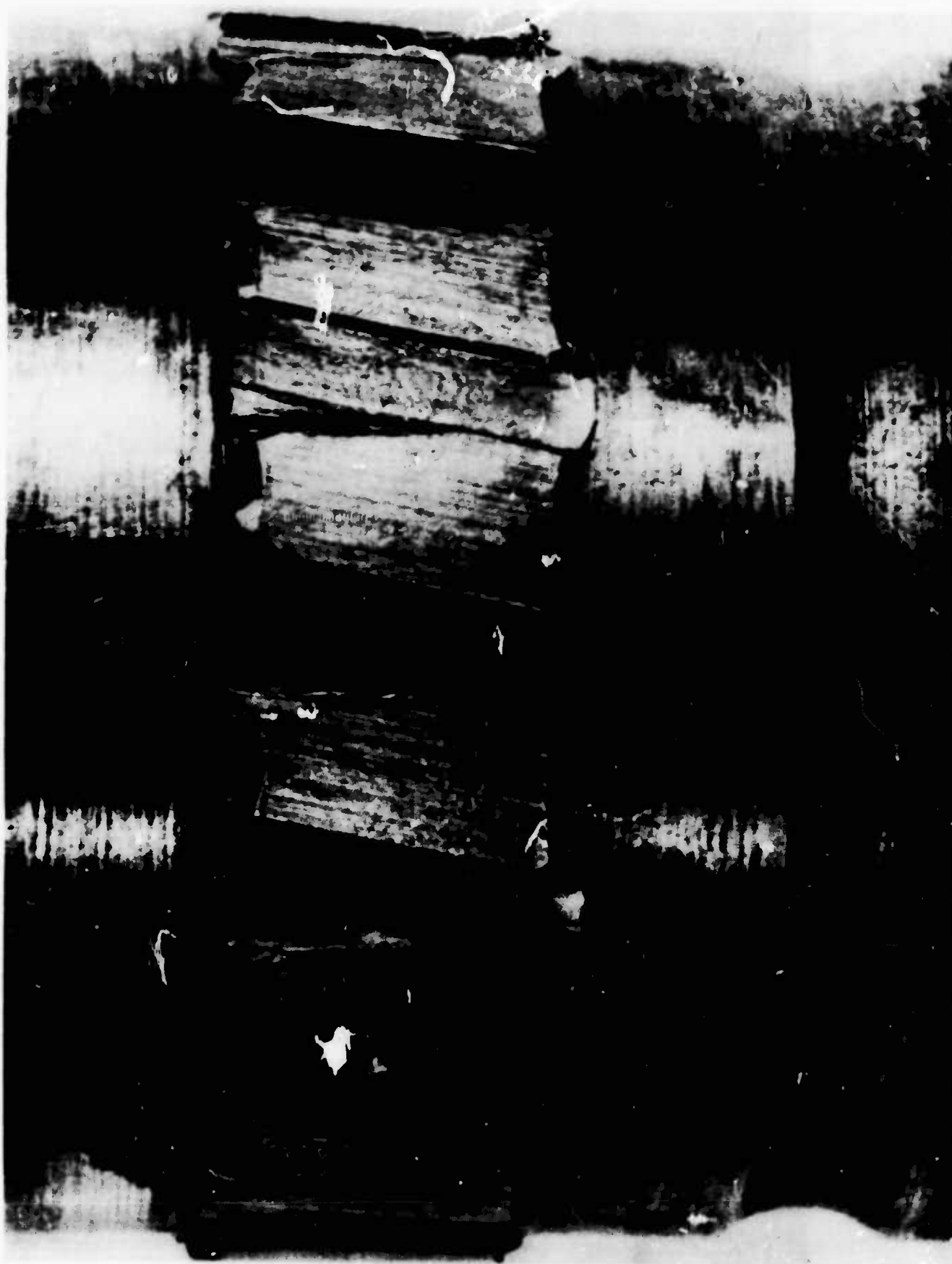
SUPERSONIC WIND TUNNELS, LAB. DEC.  
BALLISTIC RESEARCH LAB., A.P.G., MD. 1955

FIG. 3

CONFIDENTIAL

ALL DIMENSIONS ARE IN CALIBERS

**CONFIDENTIAL**



**Figure 4. Photograph of 30mm Aircraft Bullet Rotating Band Grooves.**

**CONFIDENTIAL**

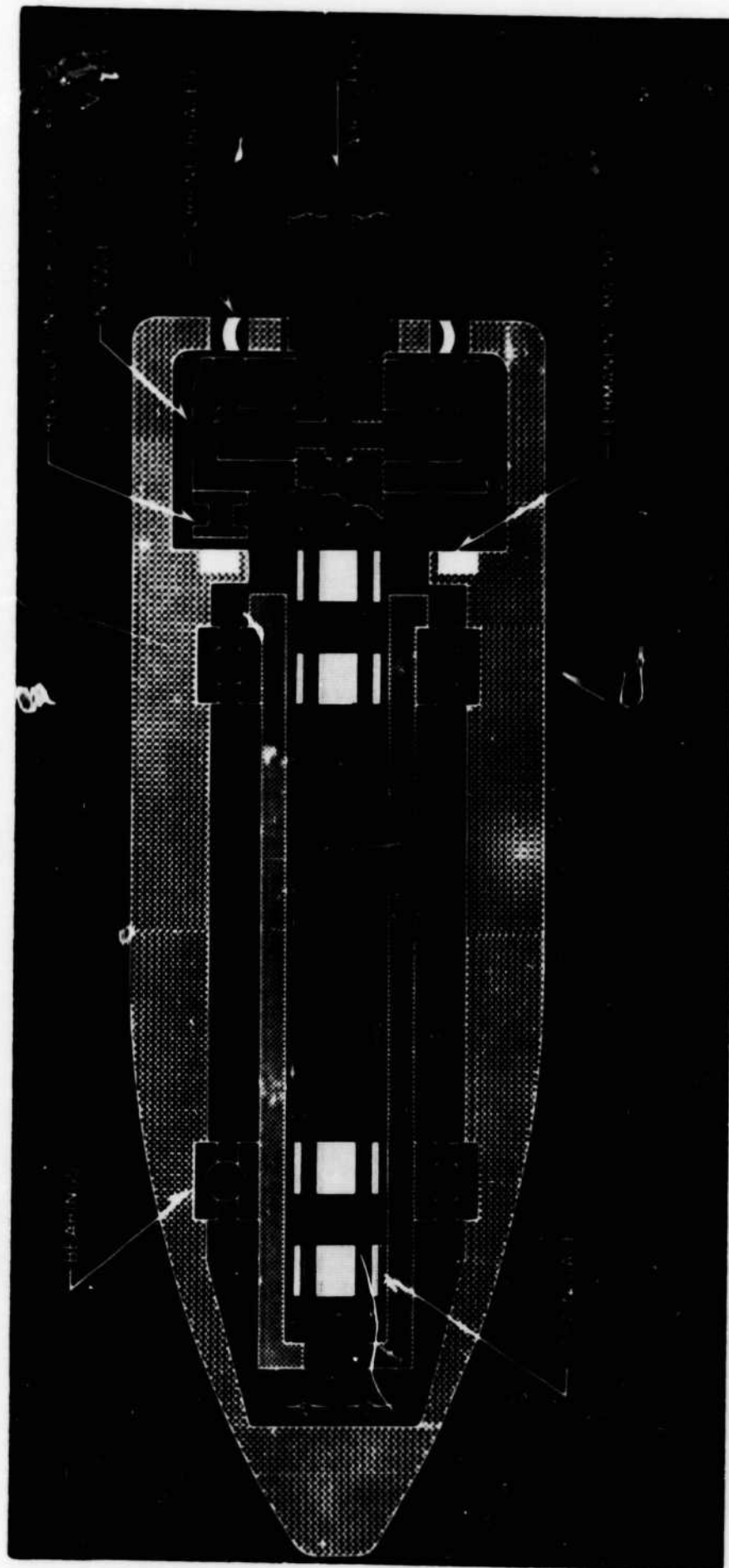


Figure 5. Spinning Model - Instrumentation.

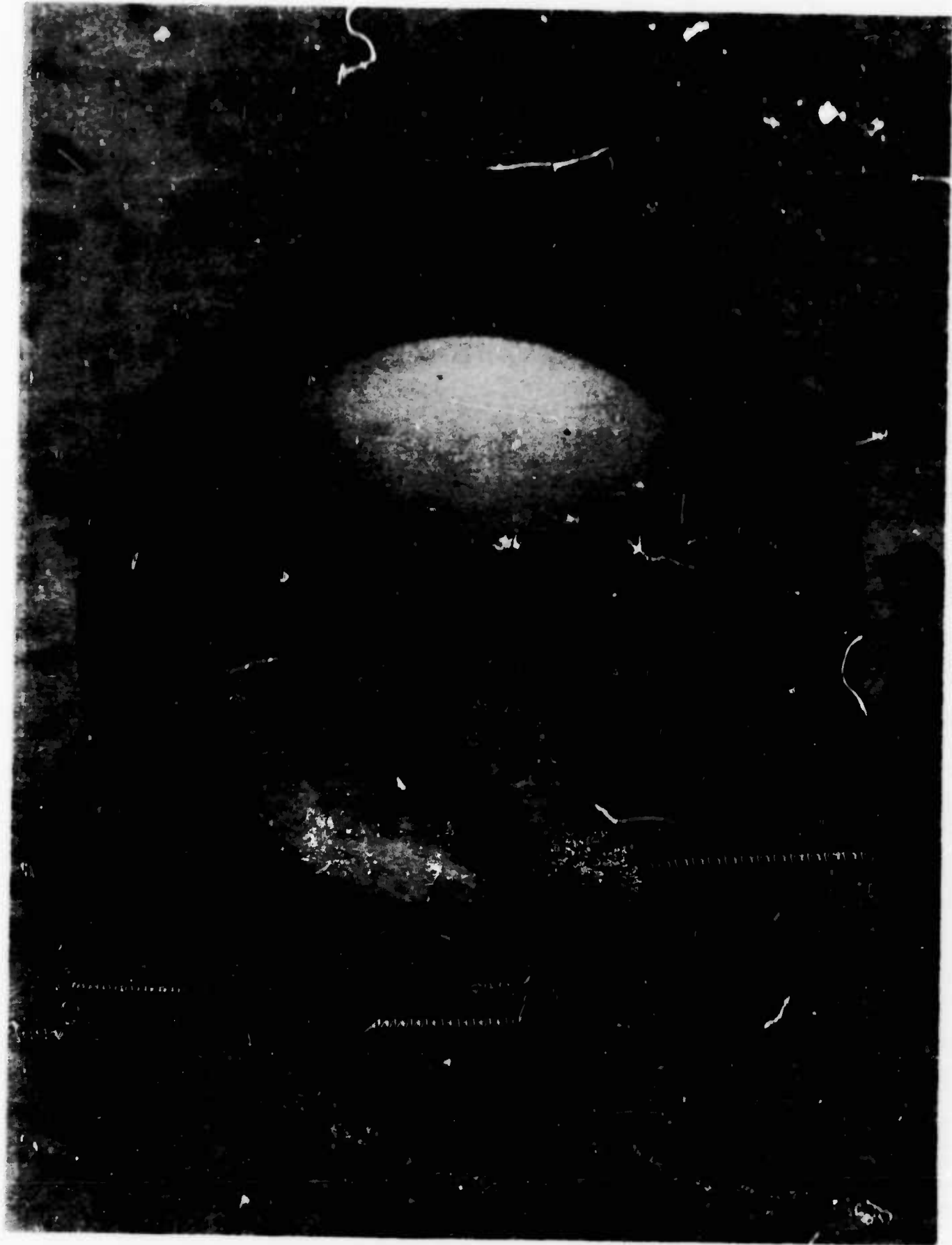


Figure 6. Ball Bearing after Break-in Period.

CONFIDENTIAL



Figure 7.

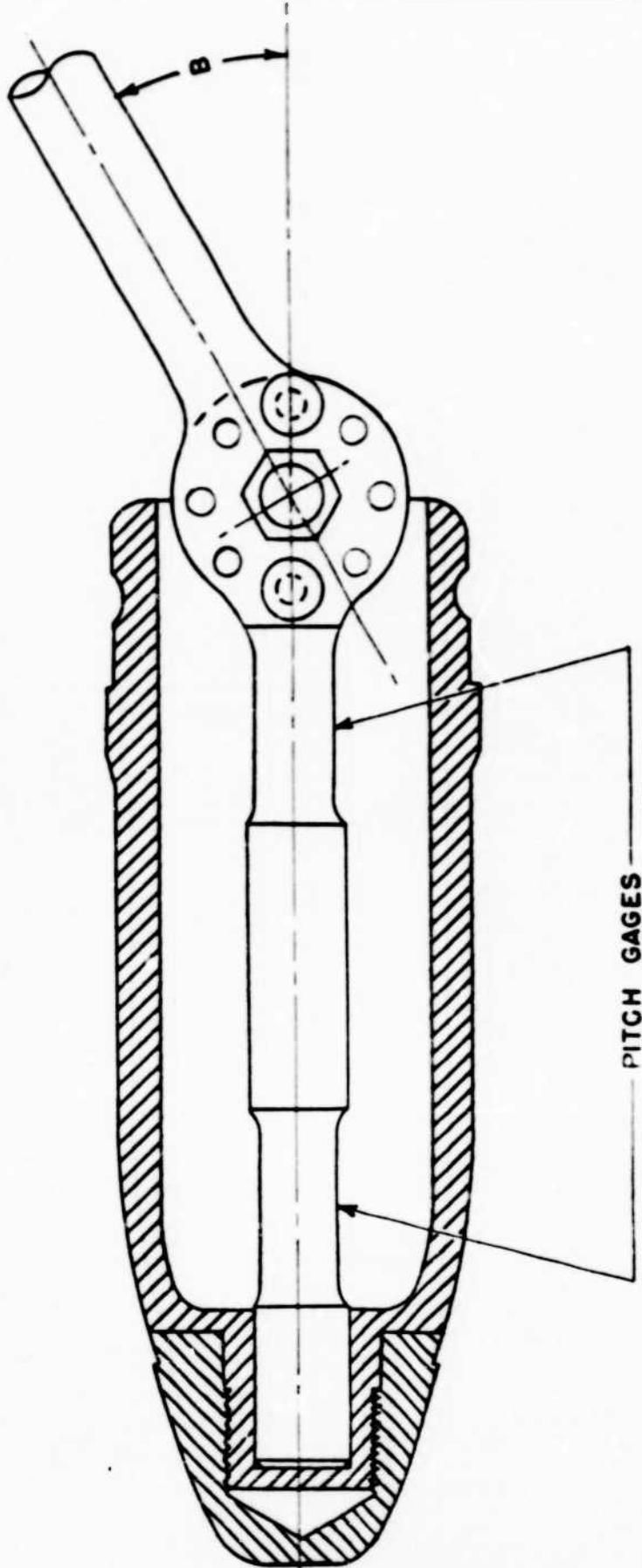


Figure 8.

CONFIDENTIAL

CONFIDENTIAL

CONFIDENTIAL



NOTE:

B CAN BE SET TO 0°, 10°, 20°, 30°

CONFIDENTIAL

FIG. 9

SUPPORT INTERFERENCE SERIES

SUPERSONIC WIND TUNNELS, LAB. DEC.  
BALLISTIC RESEARCH LAB., A.P.G., MD 1955

CONFIDENTIAL

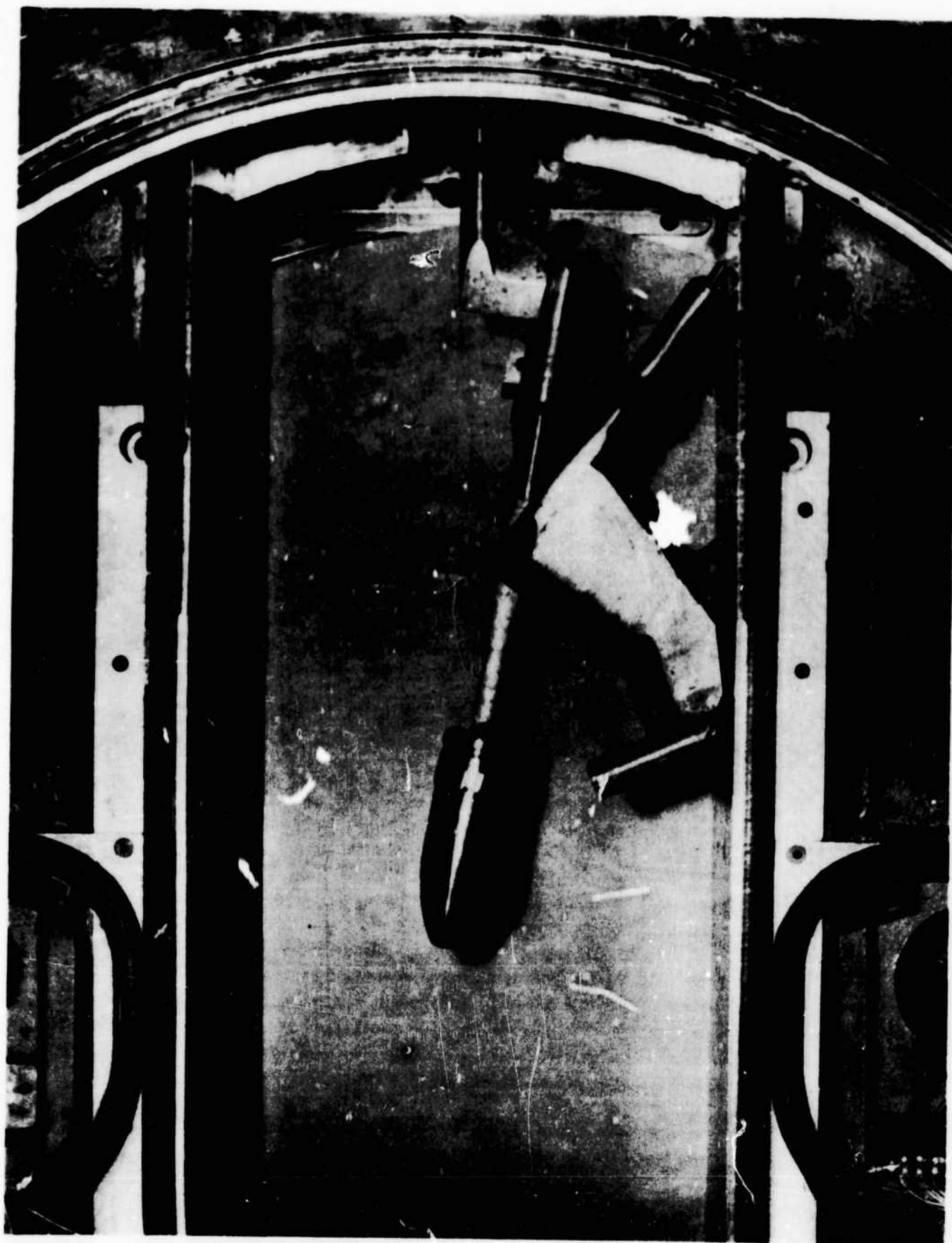


Figure 10. 30mm Aircraft Bullet Model Mount on the Tunnel Angle of Attack System showing the 10° and 32° Offset Strut Supports.



**CONFIDENTIAL**



Figure 11. Schlieren Picture of the 30mm Bullet Using a  $0^\circ$  Swept Strut,  
 $Ma = 1.57$   $\alpha = 40^\circ$ .

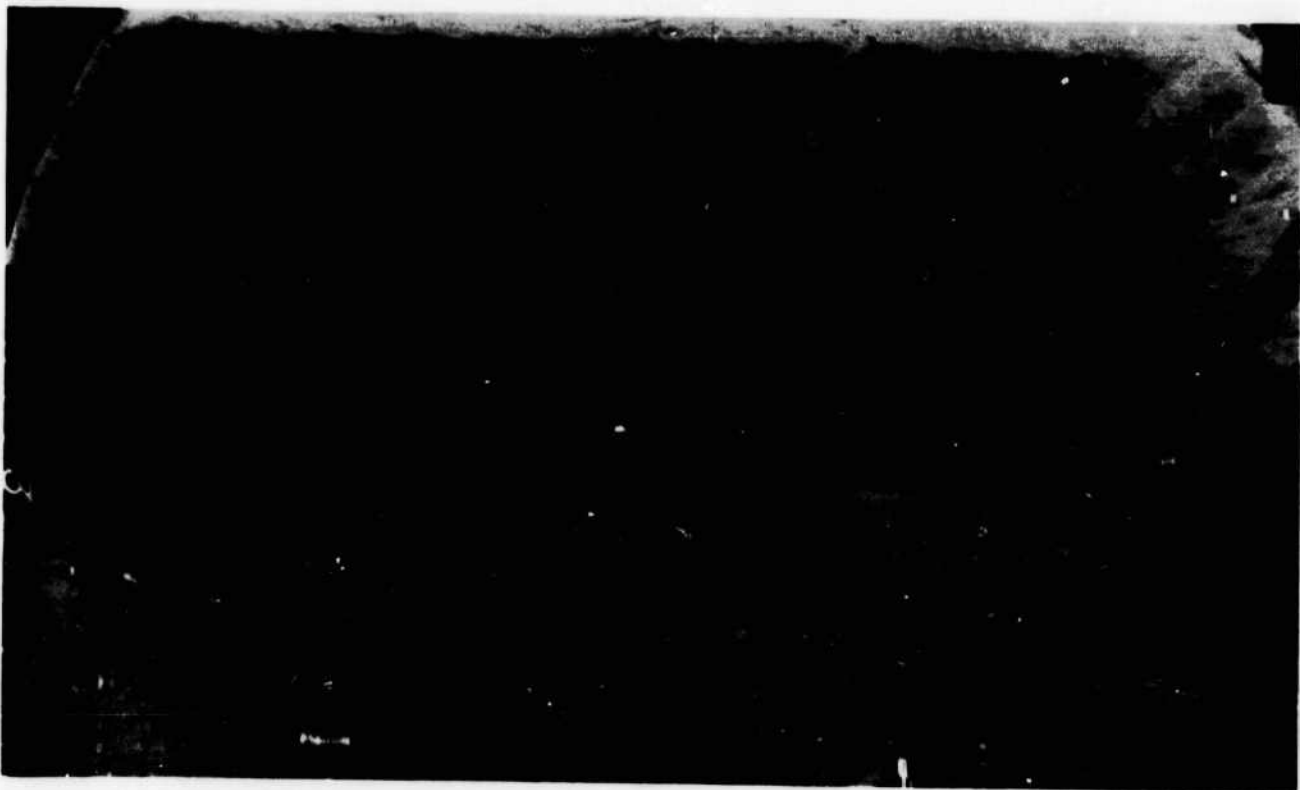


Figure 11. Schlieren Picture of the 30mm Bullet Using a  $10^\circ$  Swept Strut,  
 $Ma = 1.57$   $\alpha = 40^\circ$ .

**CONFIDENTIAL**

CONFIDENTIAL



Figure 11. Schlieren Picture of the 30mm Bullet Using a  $20^\circ$  Swept Strut,  $Ma = 1.57$   $\alpha = 40^\circ$ .



Figure 11. Schlieren Picture of the 30mm Bullet Using a  $30^\circ$  Swept Strut,  $Ma = 1.57$   $\alpha = 40^\circ$ .

CONFIDENTIAL

CONFIDENTIAL



Figure 12. Schlieren Picture of the 30mm Bullet Using a  $20^\circ$  Swept Strut,  
 $Ma = 1.57$   $\alpha = 30^\circ$ .



Figure 12. Schlieren Picture of the 30mm Bullet Using a  $30^\circ$  Swept Strut,  
 $Ma = 1.57$   $\alpha = 30^\circ$ .

CONFIDENTIAL

CONFIDENTIAL

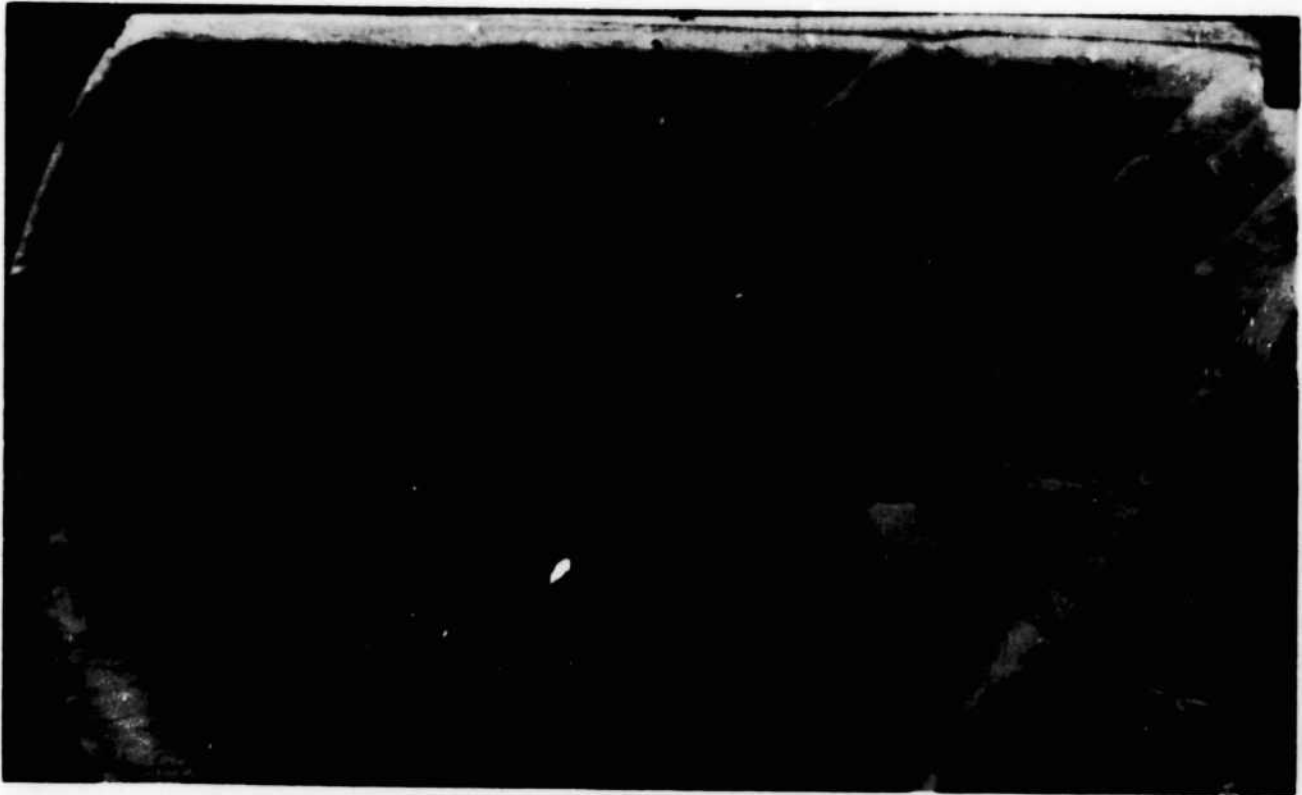


Figure 12. Schlieren Picture of the 30mm Bullet Using a  $0^\circ$  Swept Strut,  
 $Ma = 1.57$   $\alpha = 30^\circ$ .

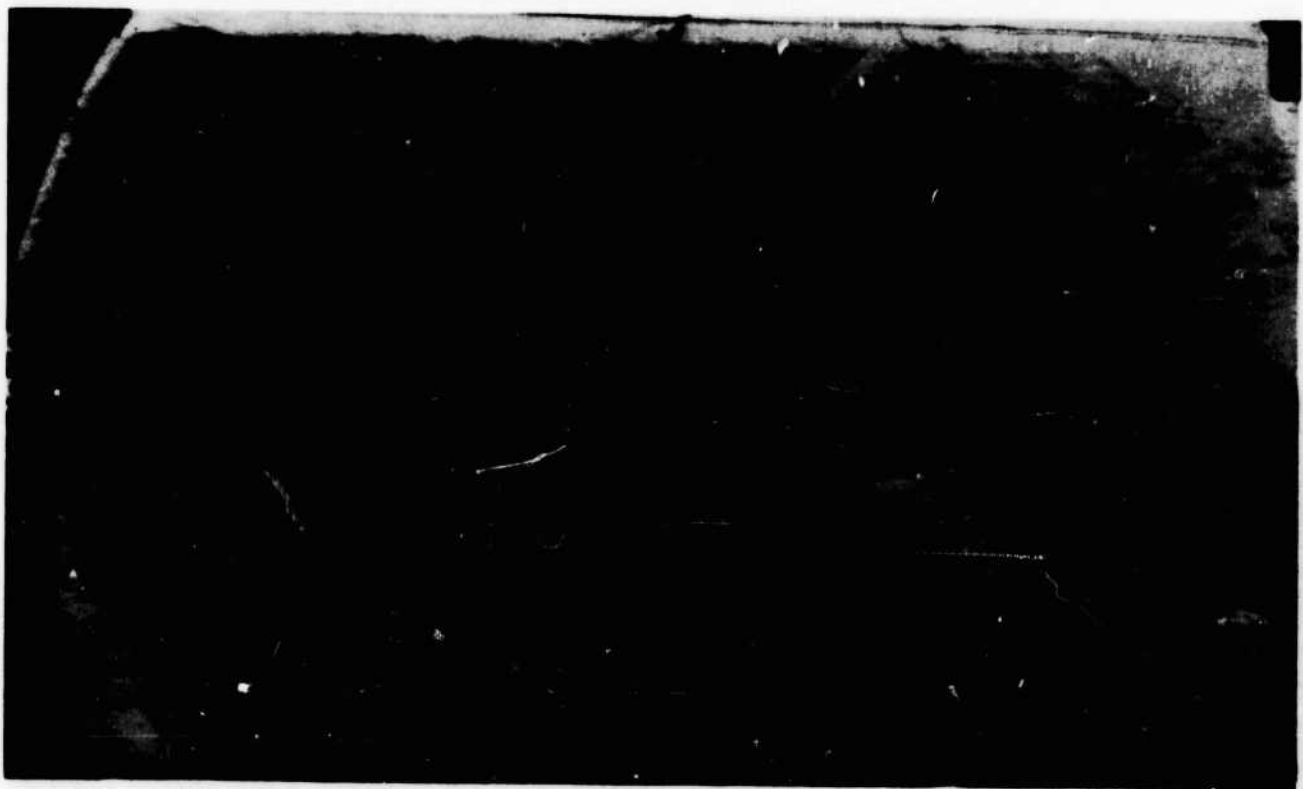
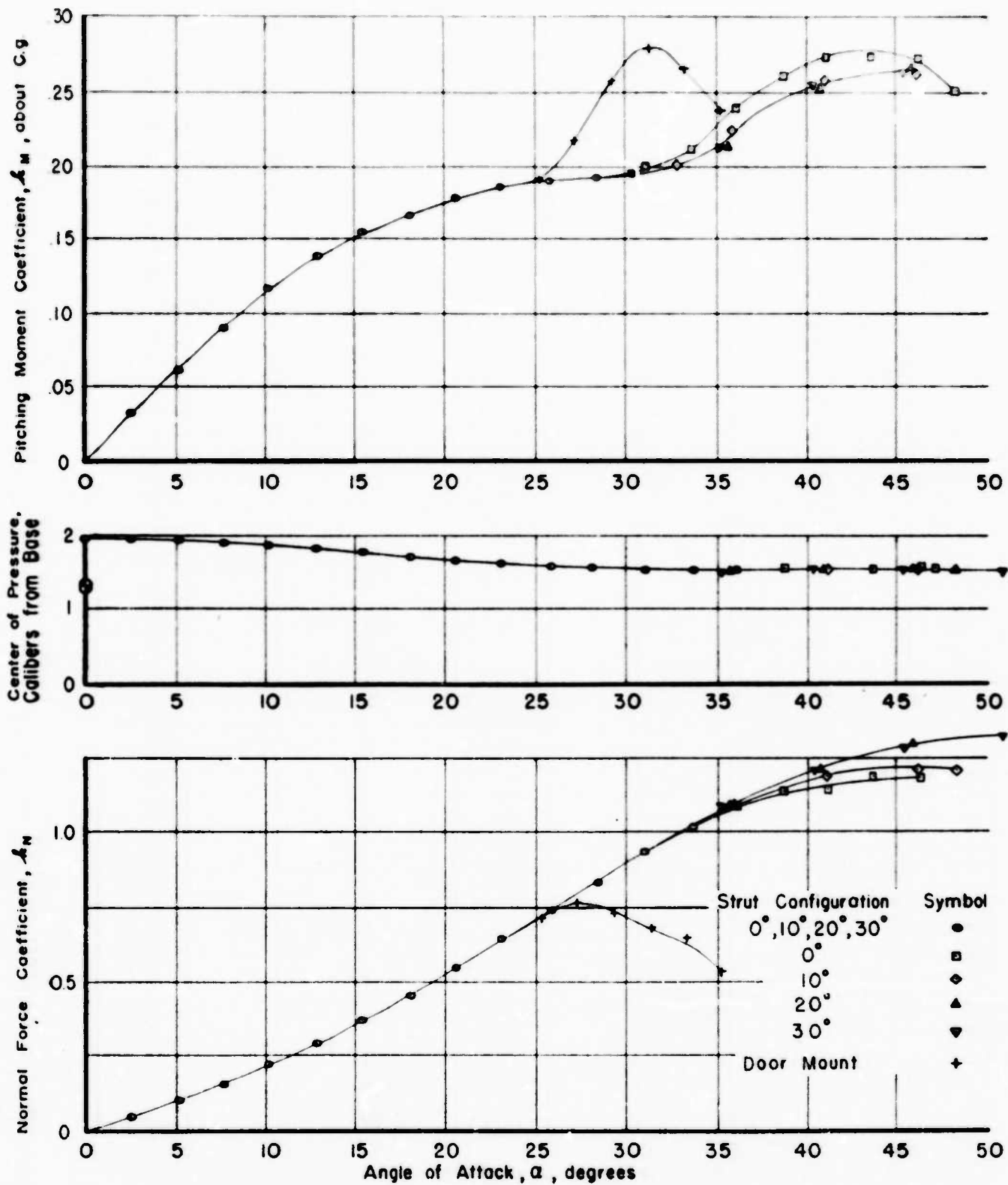


Figure 12. Schlieren Picture of the 30mm Bullet Using a  $10^\circ$  Swept Strut,  
 $Ma = 1.57$   $\alpha = 30^\circ$ .

CONFIDENTIAL

CONFIDENTIAL



SUPPORT AND TUNNEL INTERFERENCE

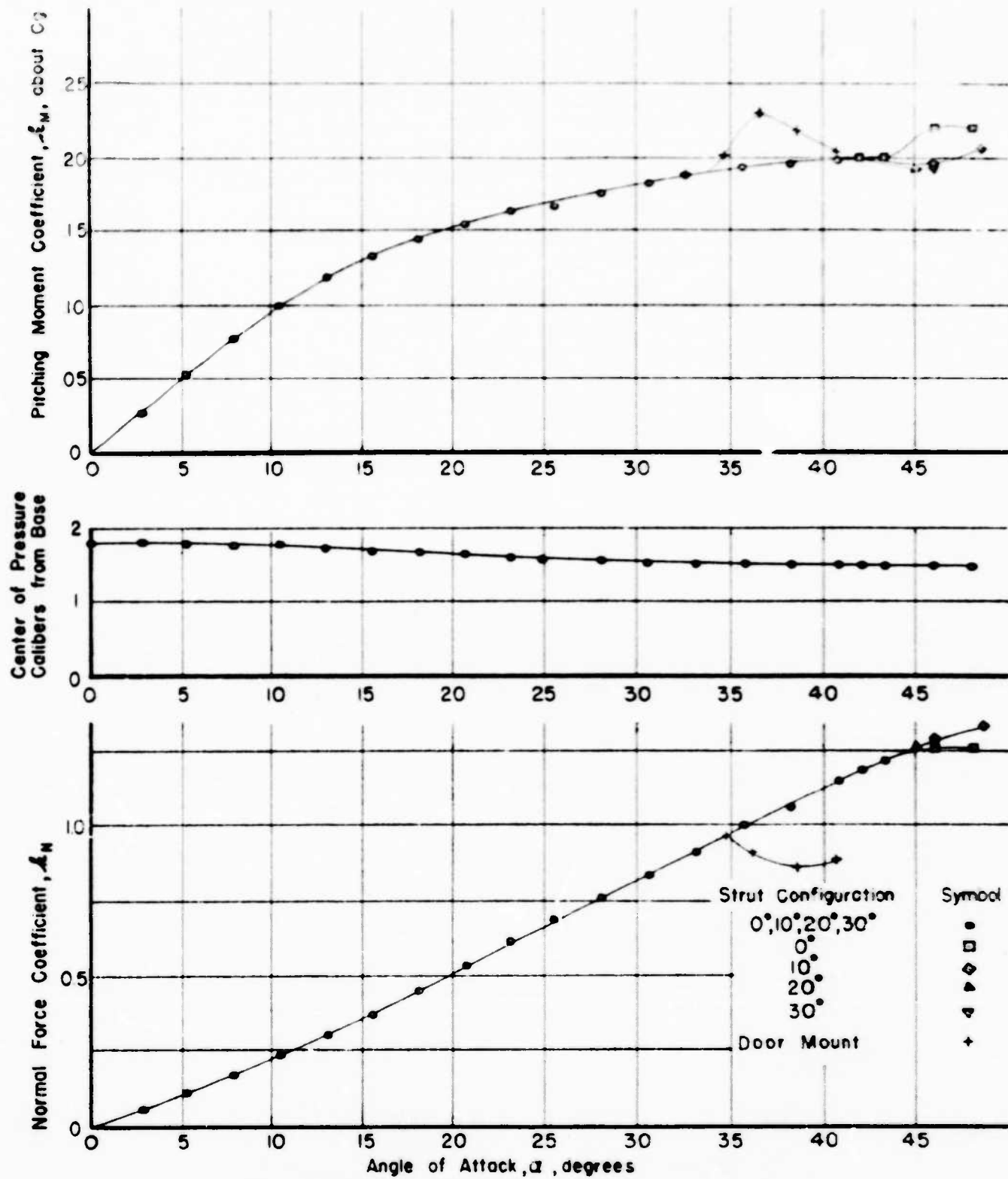
Mo = 1.57

Re =  $84 \times 10^6$

FIG.13

CONFIDENTIAL

CONFIDENTIAL



# SUPPORT AND TUNNEL INTERFERENCE

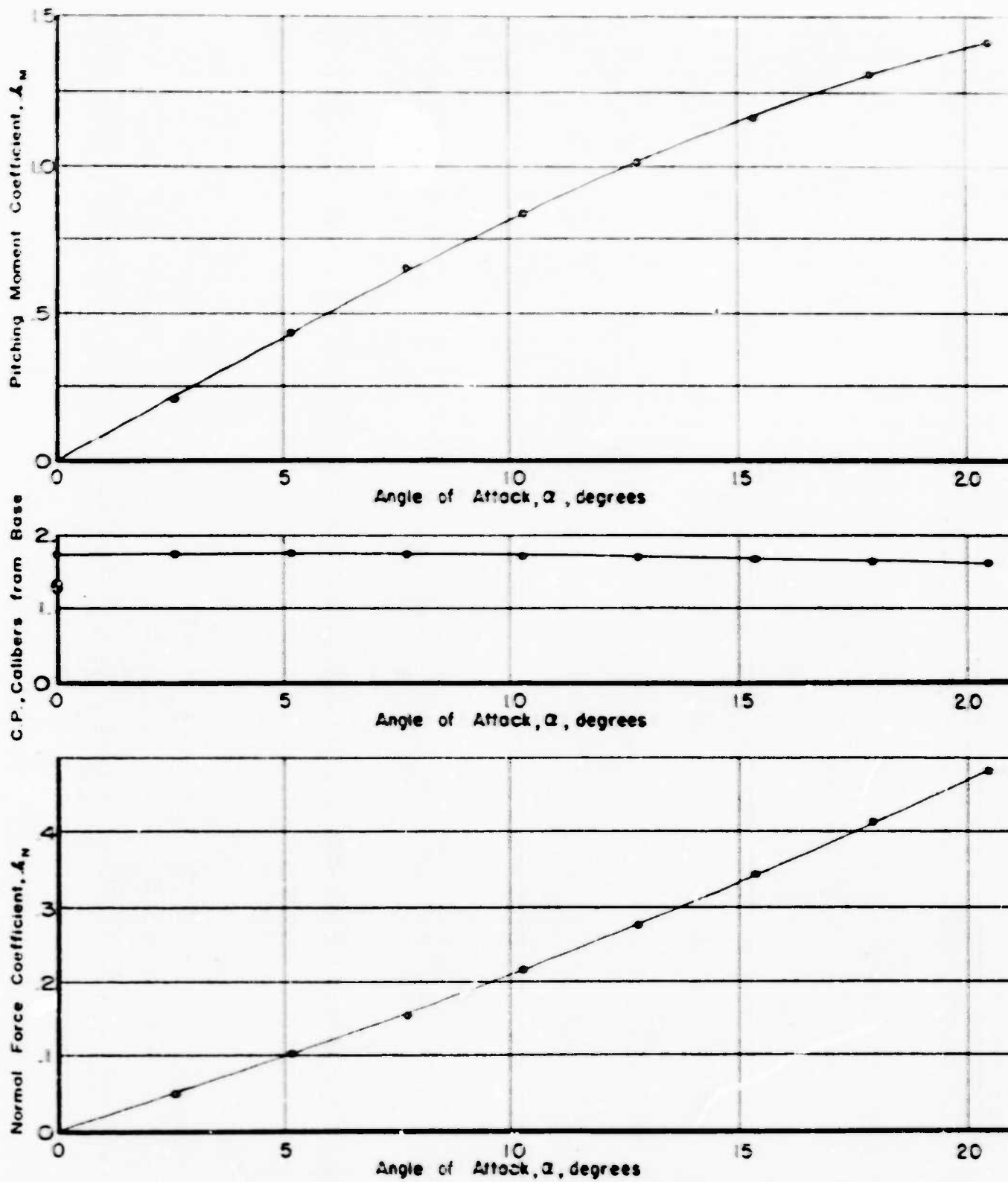
$Mo = 2.00$

$Re = 71 \times 10^6$

FIG. 14

CONFIDENTIAL

CONFIDENTIAL



PITCH DATA FOR 30 MM BULLET

$Ma = 2.47$

$Re = 76 \times 10^6$

FIG 15

CONFIDENTIAL

CONFIDENTIAL

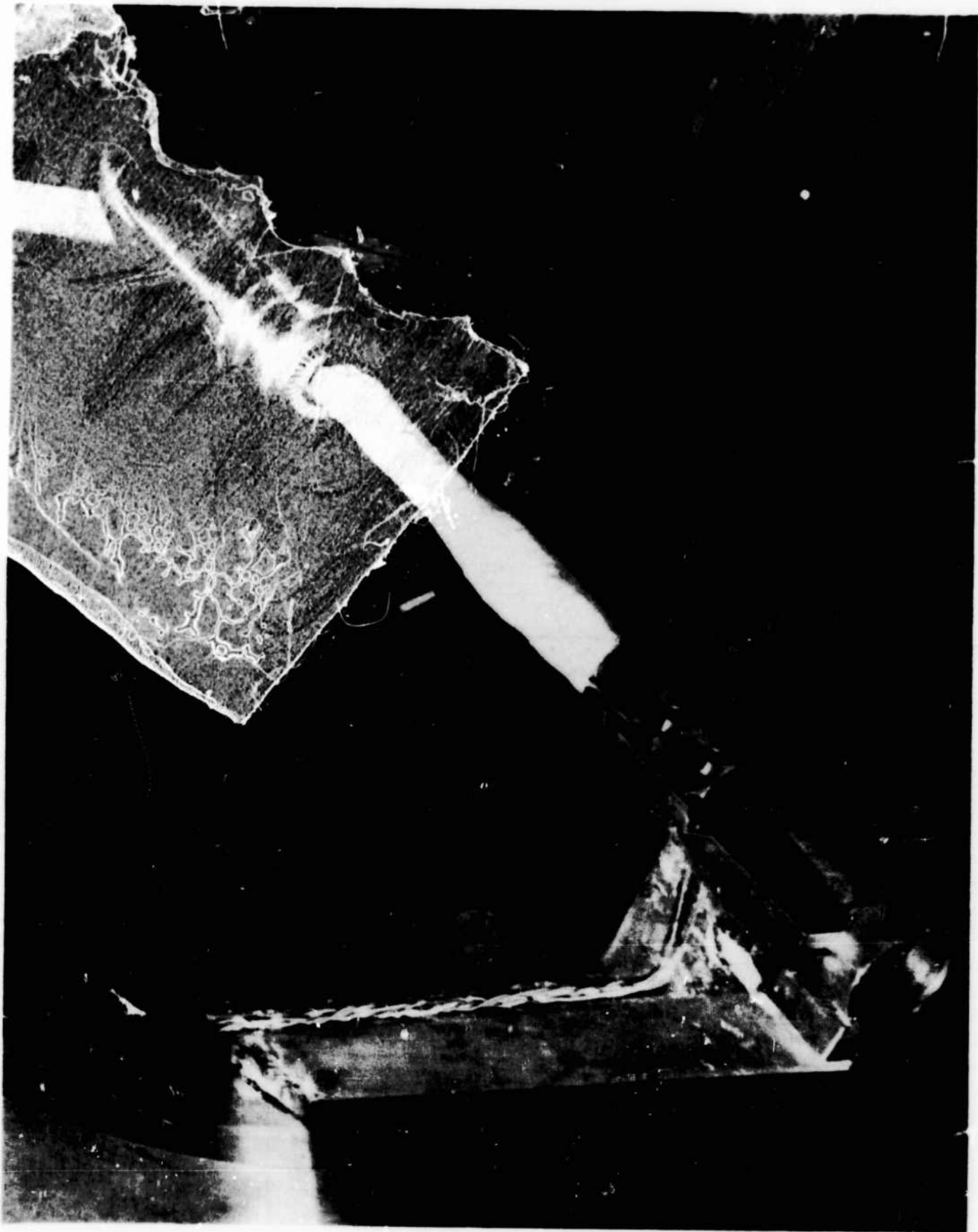
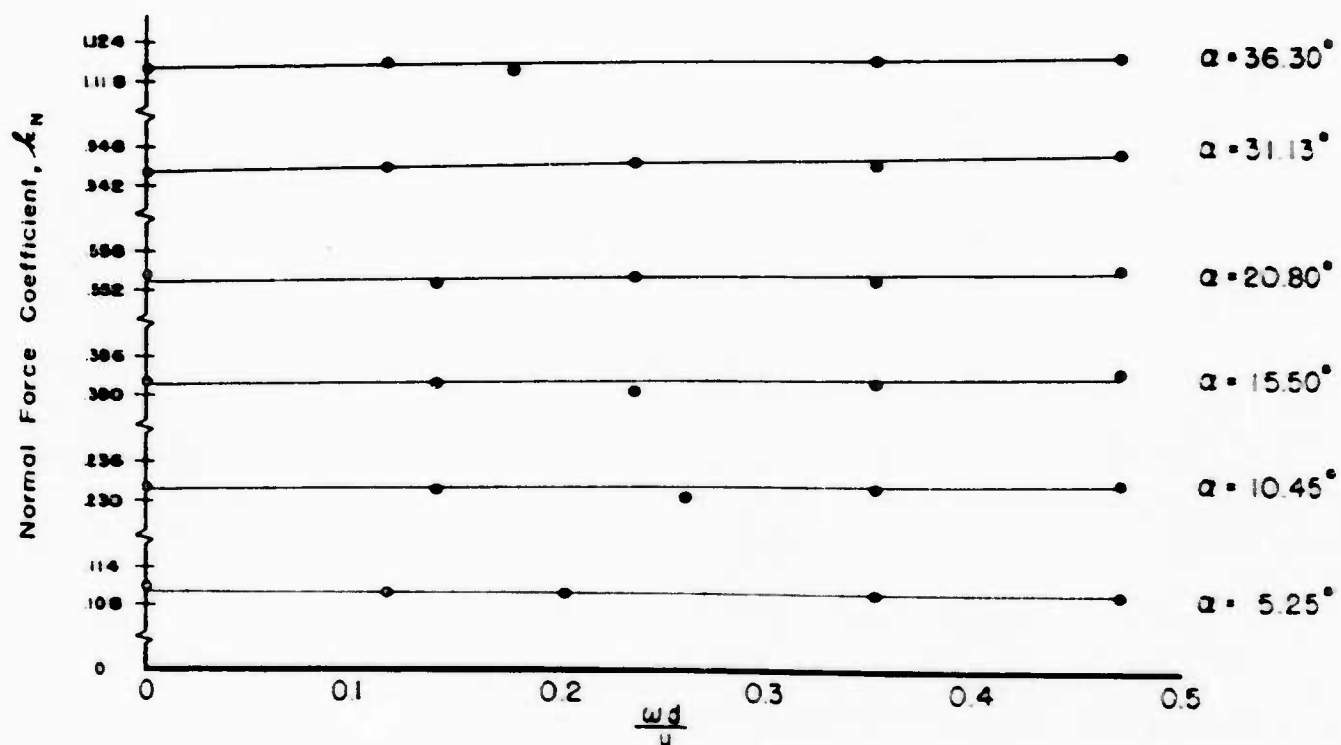
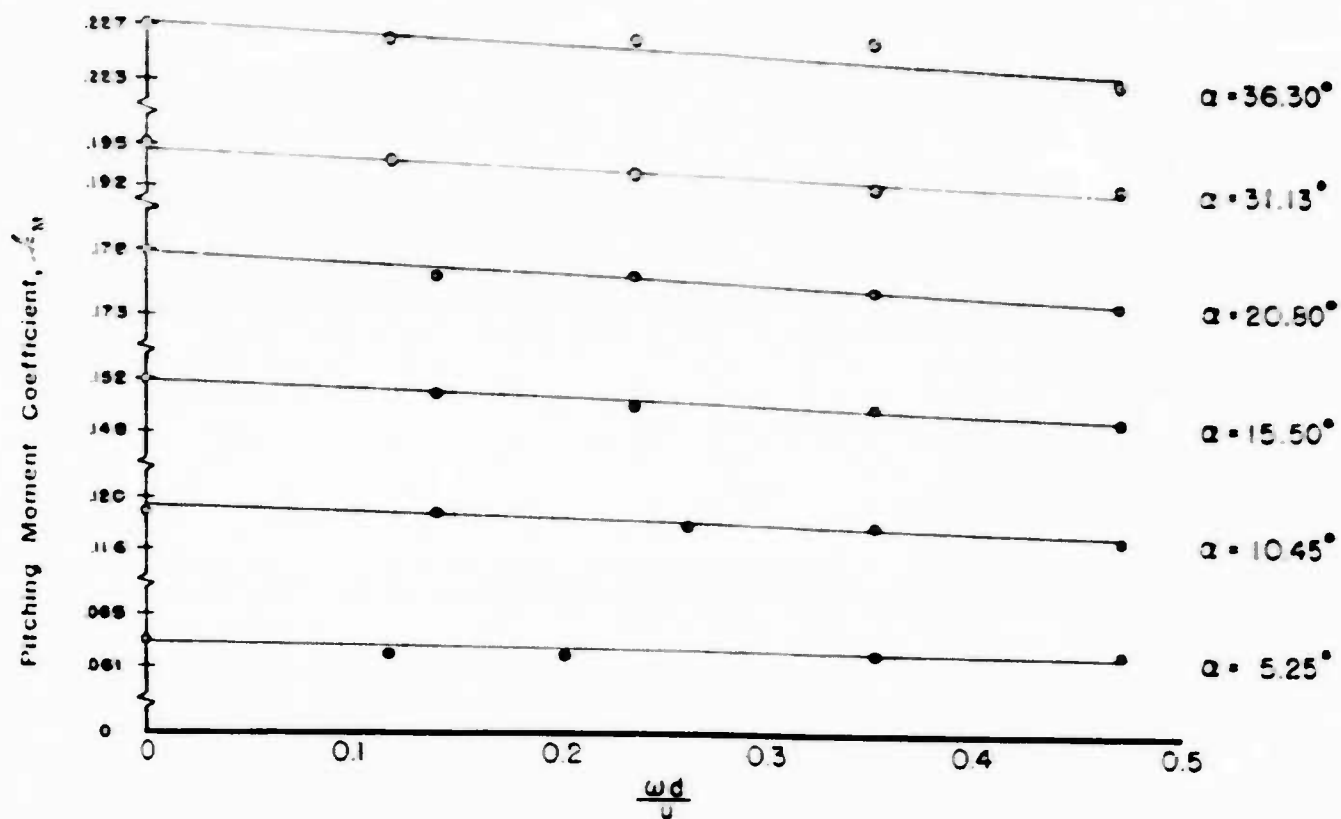


Figure 16. 2" Dia. Spinning Model Mounted on the Original Door Mount.

CONFIDENTIAL



CONFIDENTIAL



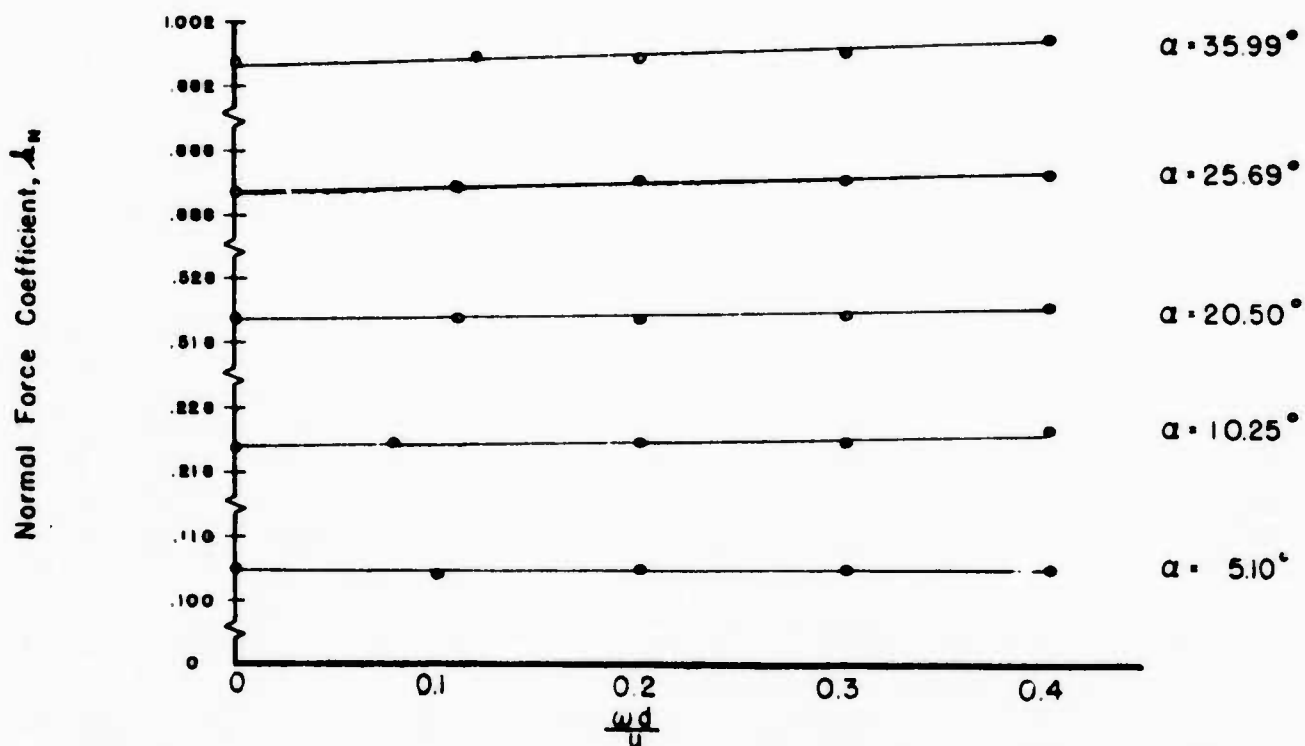
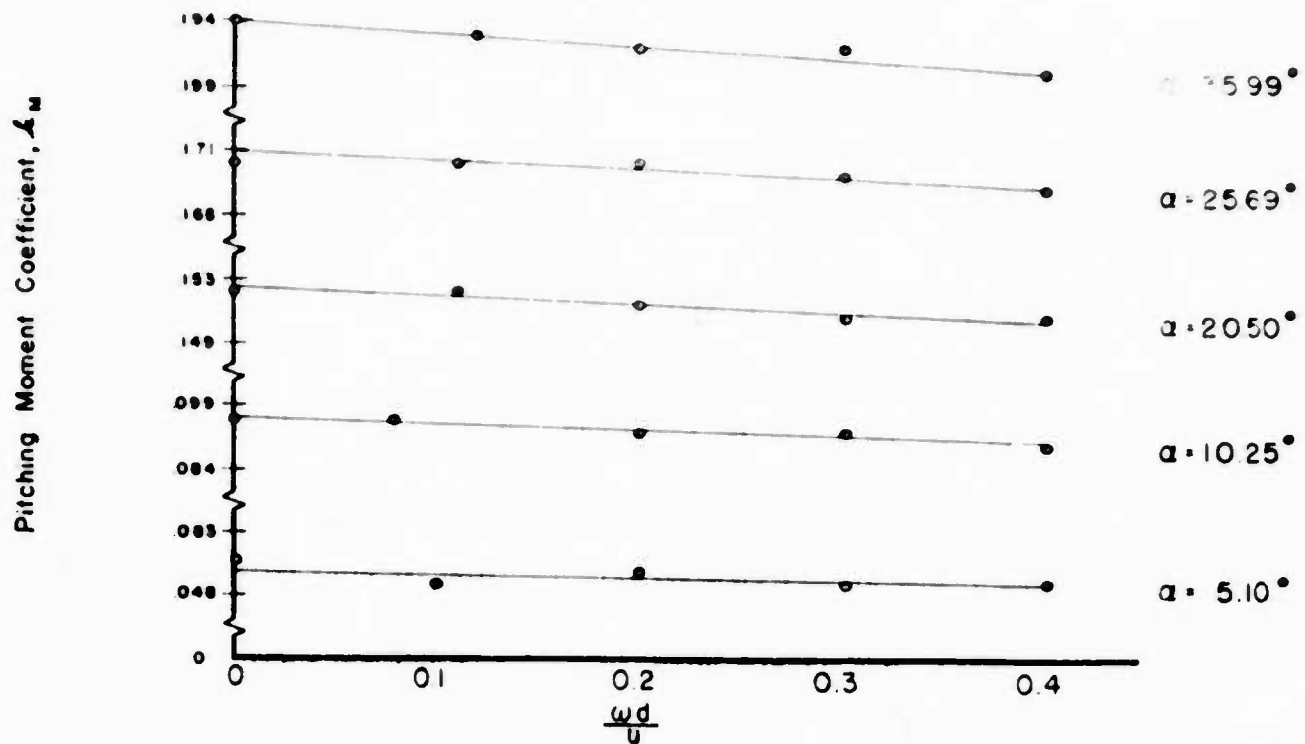
PITCH DATA VARIATION WITH SPIN FOR 30 MM BULLET

$Ma = 1.57$

$Re = 75 \times 10^6$  FIG. 17

CONFIDENTIAL

CONFIDENTIAL



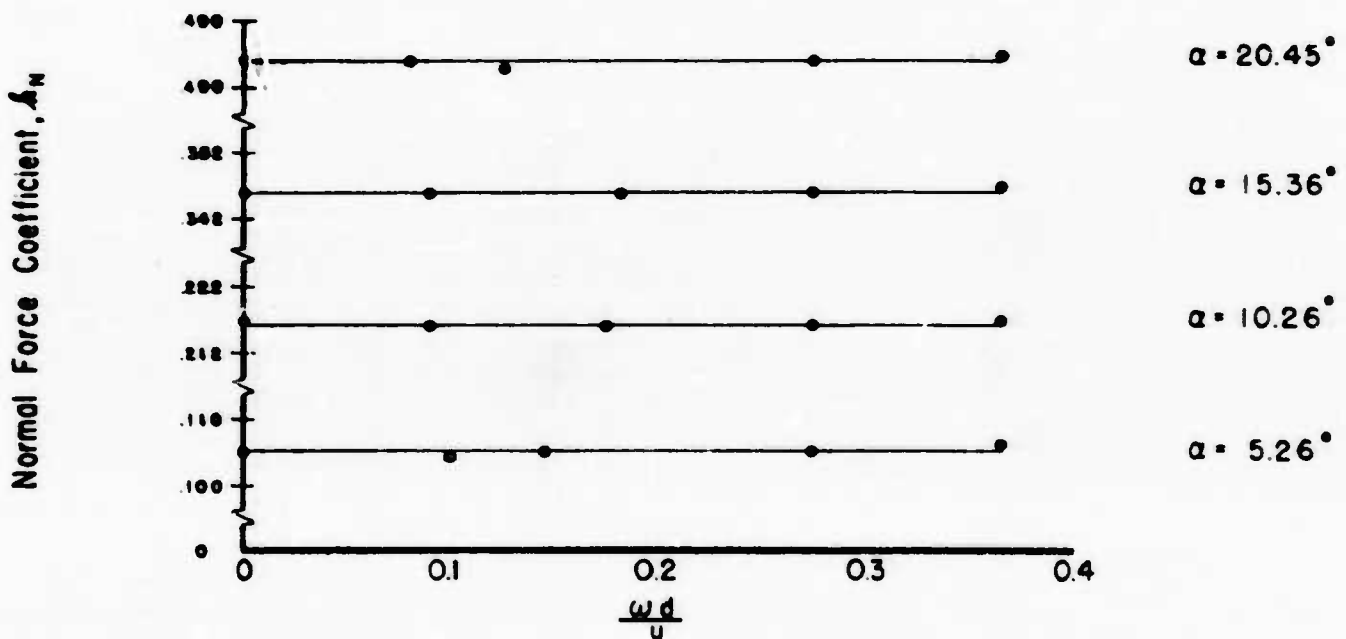
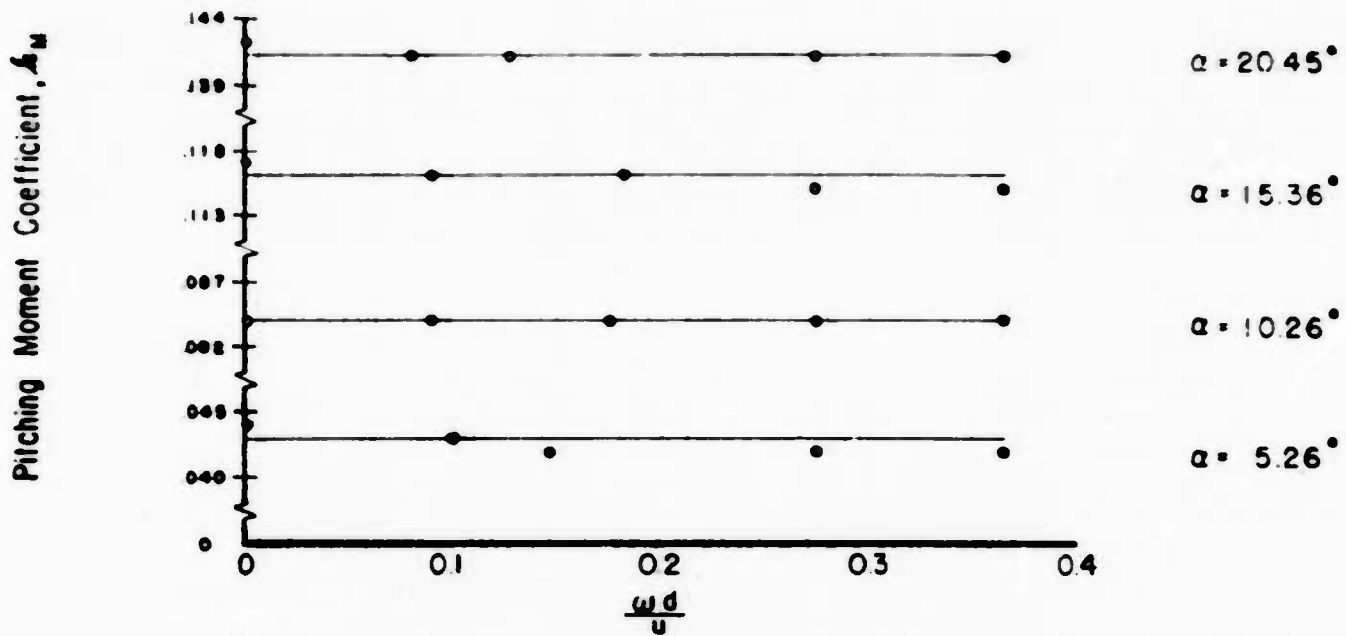
PITCH DATA VARIATION WITH SPIN FOR 30 MM BULLET

$Ma = 2.00$

$Re = .62 \times 10^6$  FIG. 18

CONFIDENTIAL

CONFIDENTIAL



PITCH DATA VARIATION WITH SPIN FOR 30 MM BULLET

$M_0 = 2.47$

$Re = .76 \times 10^6$  FIG. 19

CONFIDENTIAL

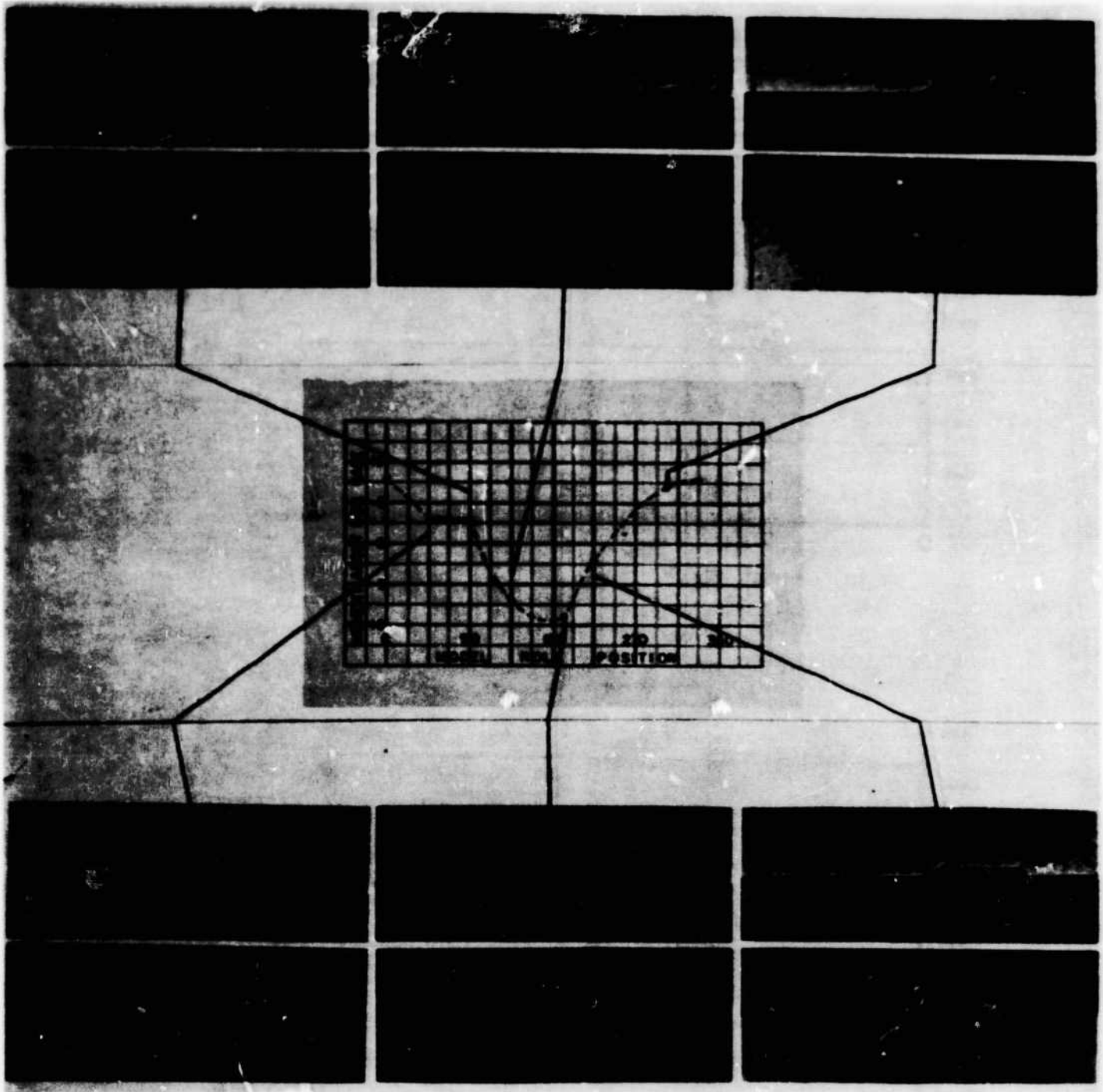


Figure 20. Illustration of Zero Shift at  $Re. = .62 \times 10^6$ .

CONFIDENTIAL

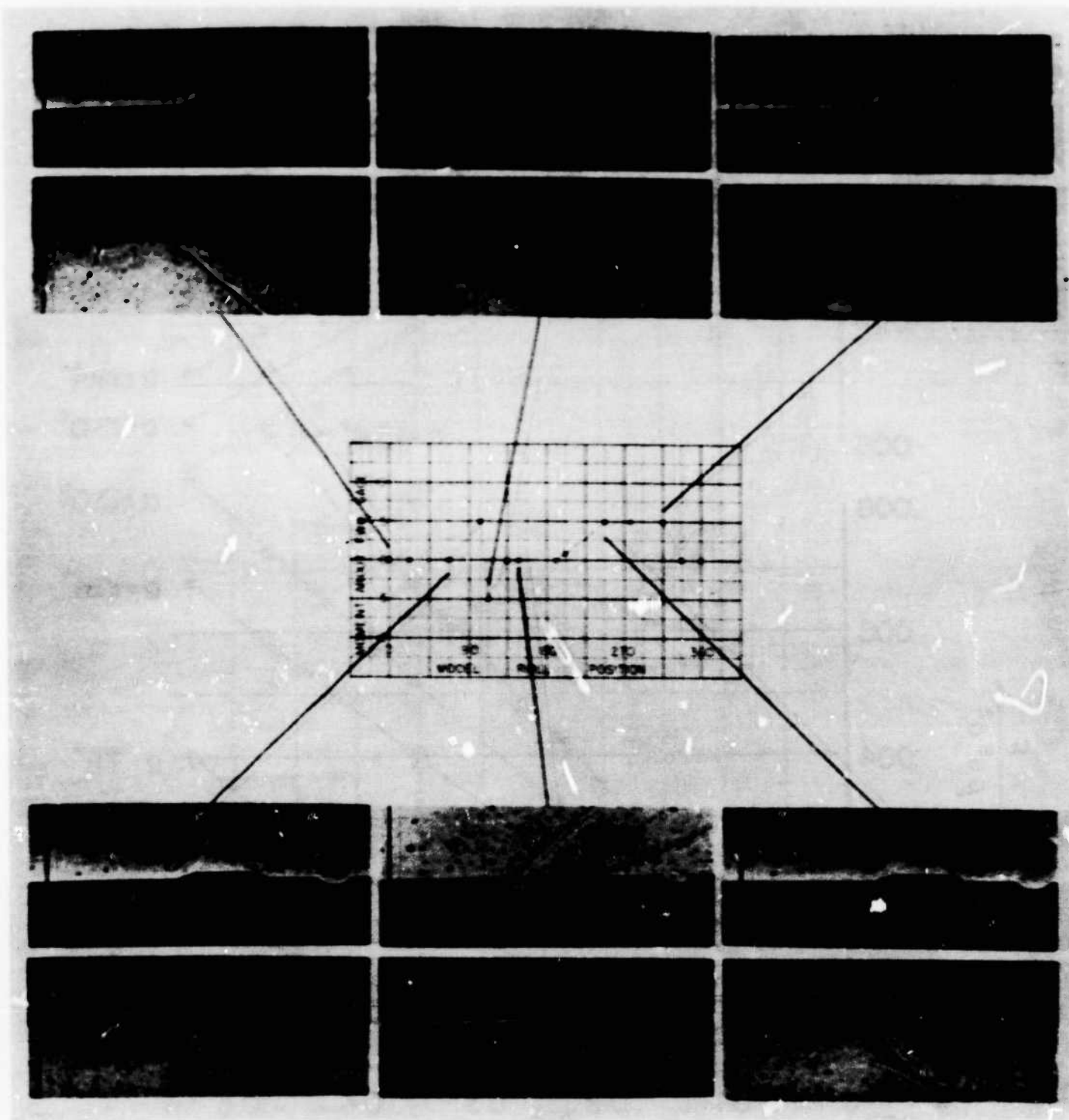
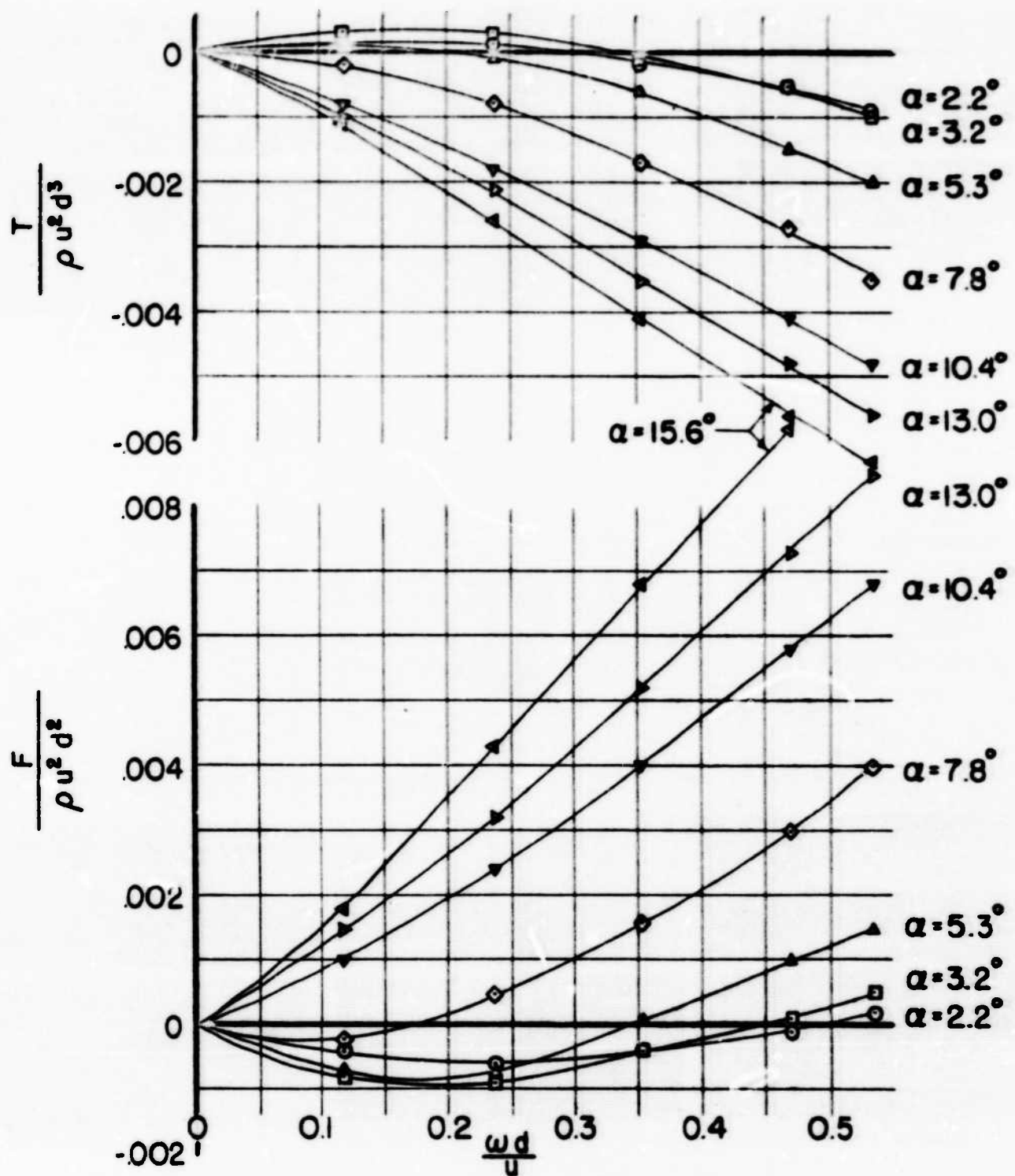


Figure 21. Illustration of Zero Shift at  $Re. = .94 \times 10^6$ .

CONFIDENTIAL



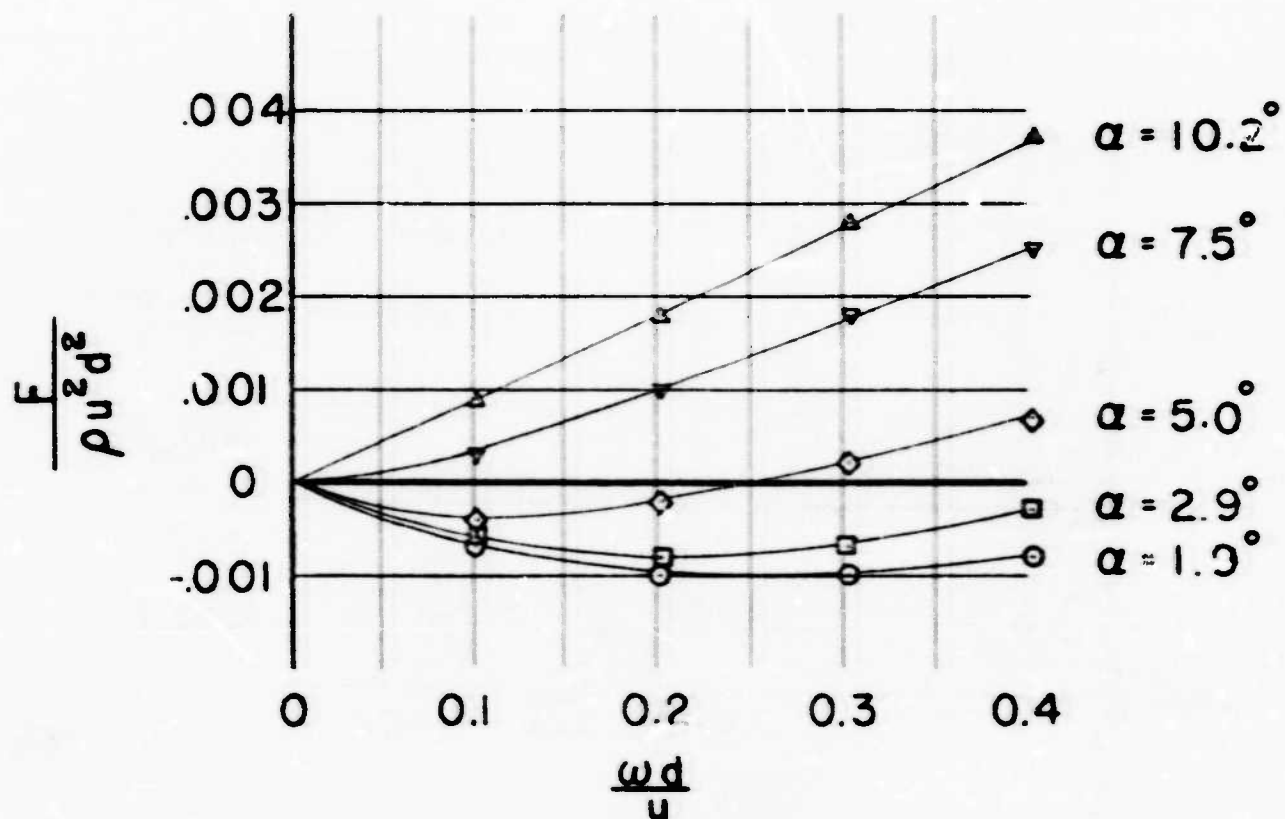
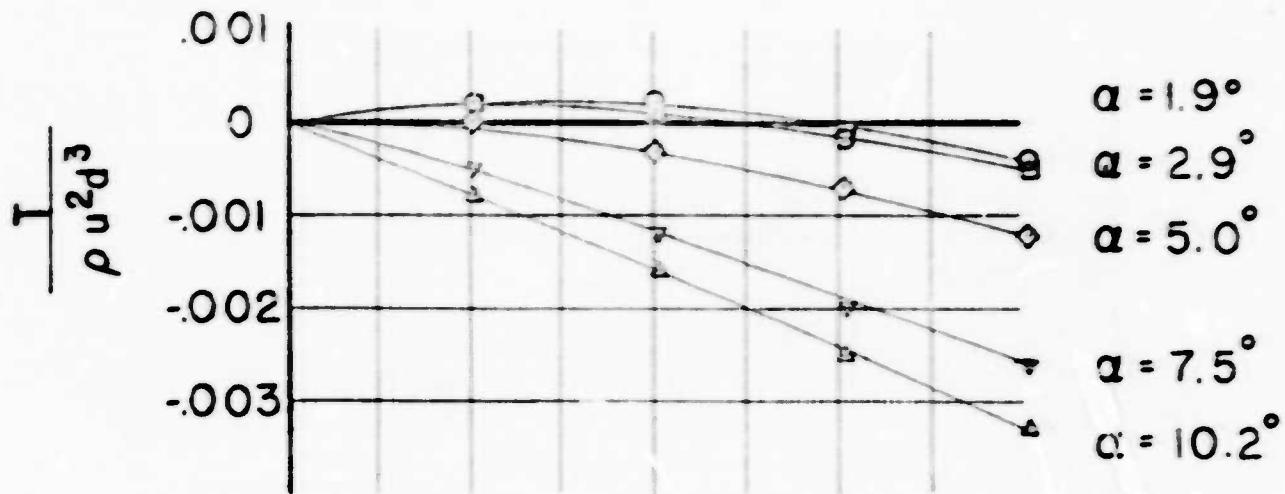
MAGNUS DATA FOR 30 MM BULLET

$Ma = 1.57$

FIG. 22

$Re = .75 \times 10^6$

CONFIDENTIAL



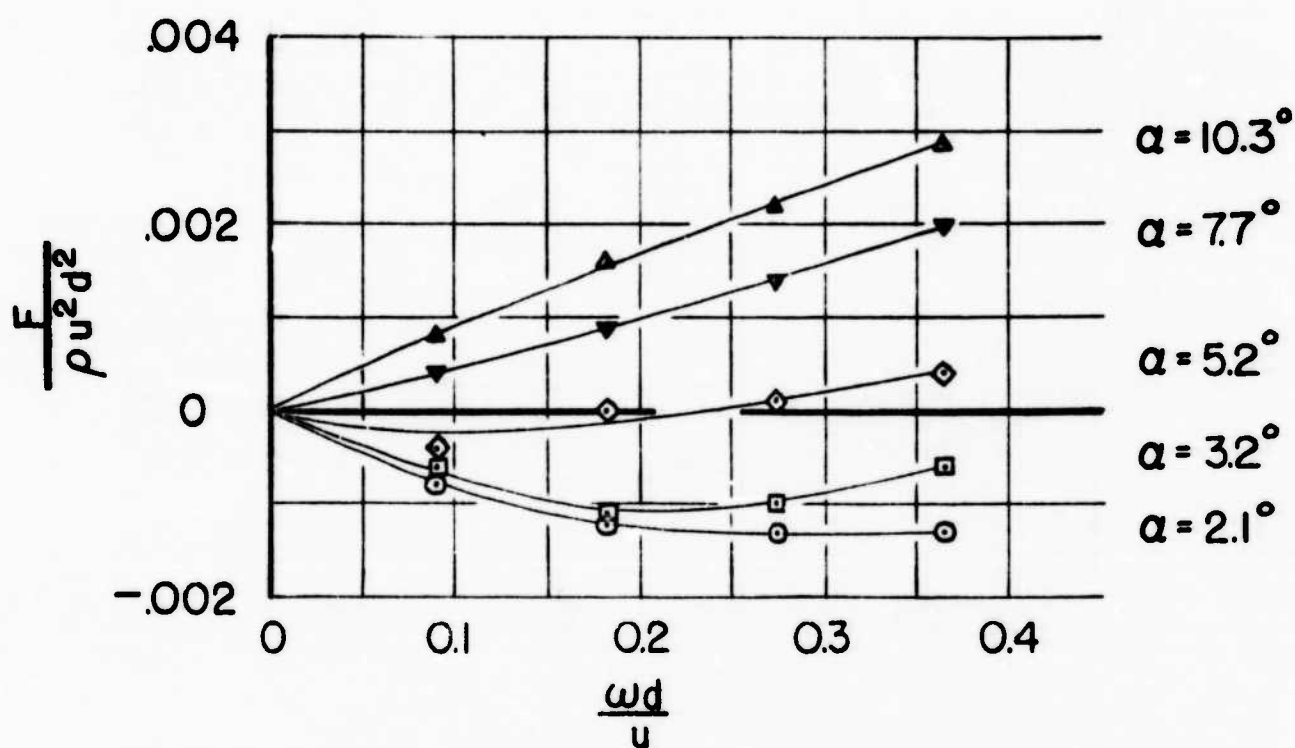
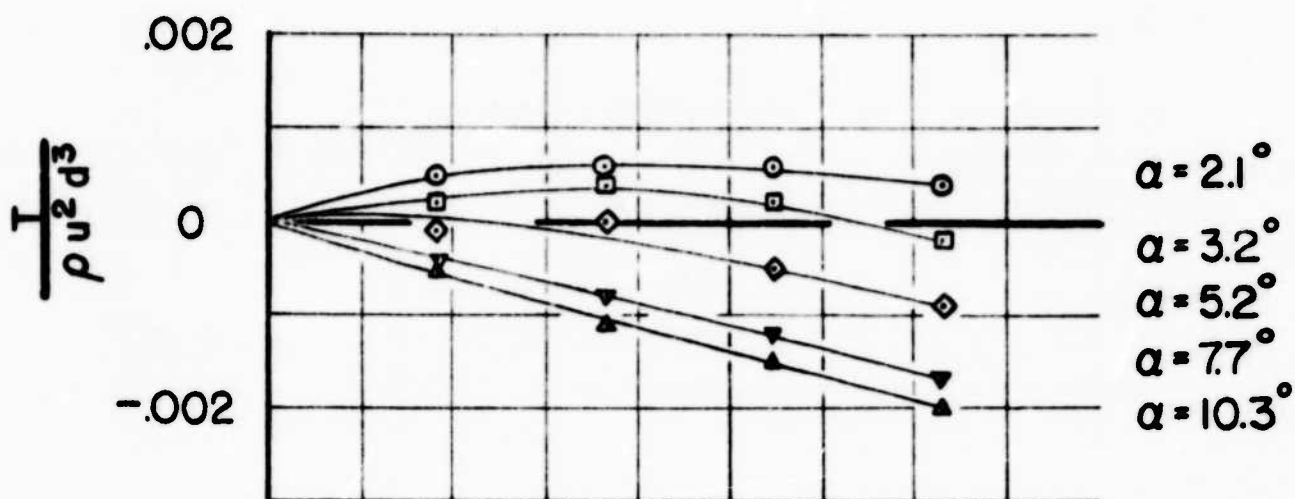
# MAGNUS DATA FOR 30 MM BULLET

Ma=2.00

FIG. 23

Re=.94 x 10<sup>6</sup>

CONFIDENTIAL



MAGNUS DATA FOR 30 MM BULLET

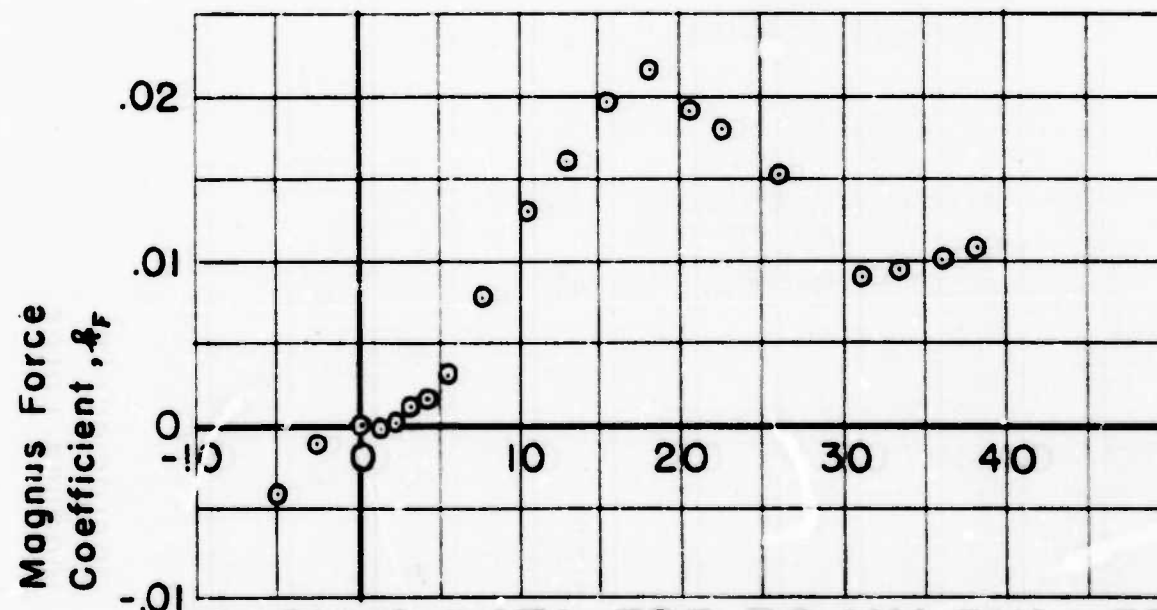
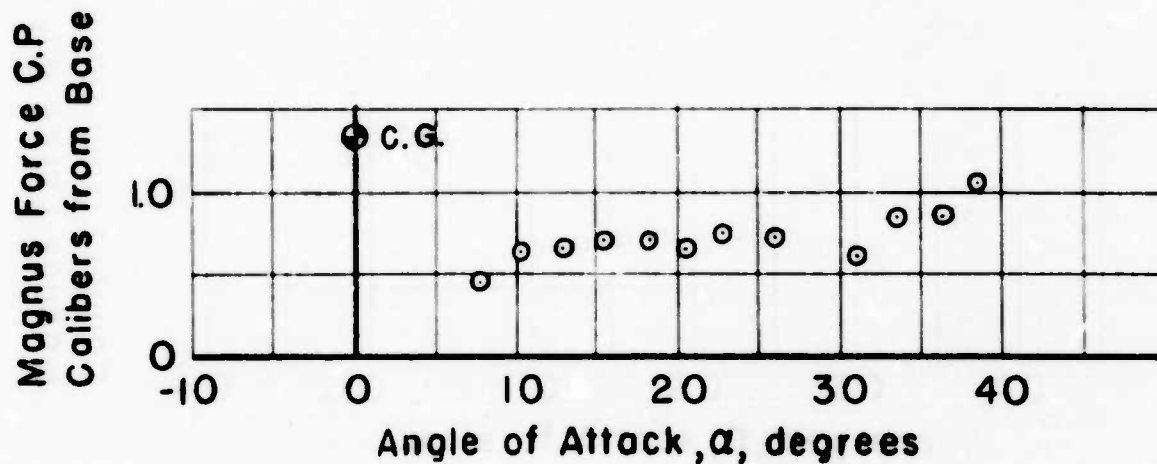
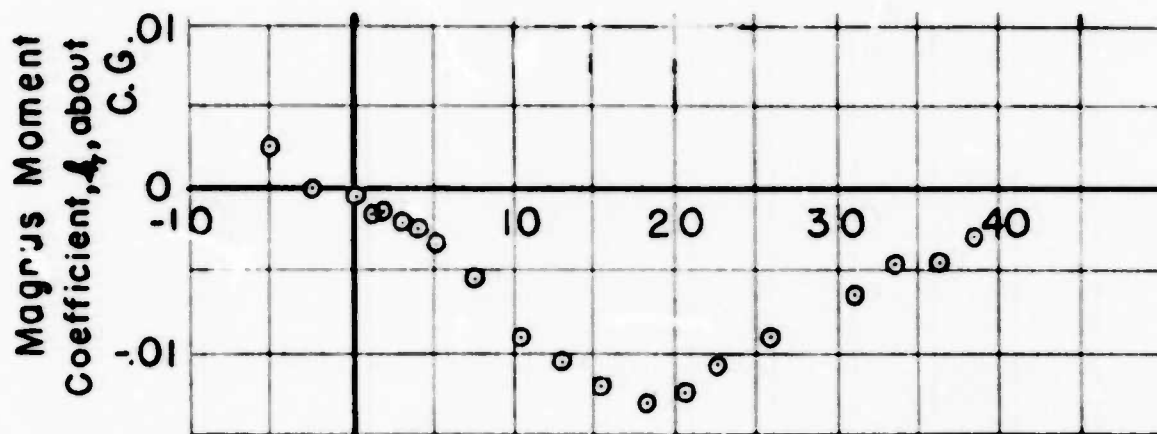
Ma = 2.47

FIG. 24

Re =  $.76 \times 10^6$



CONFIDENTIAL



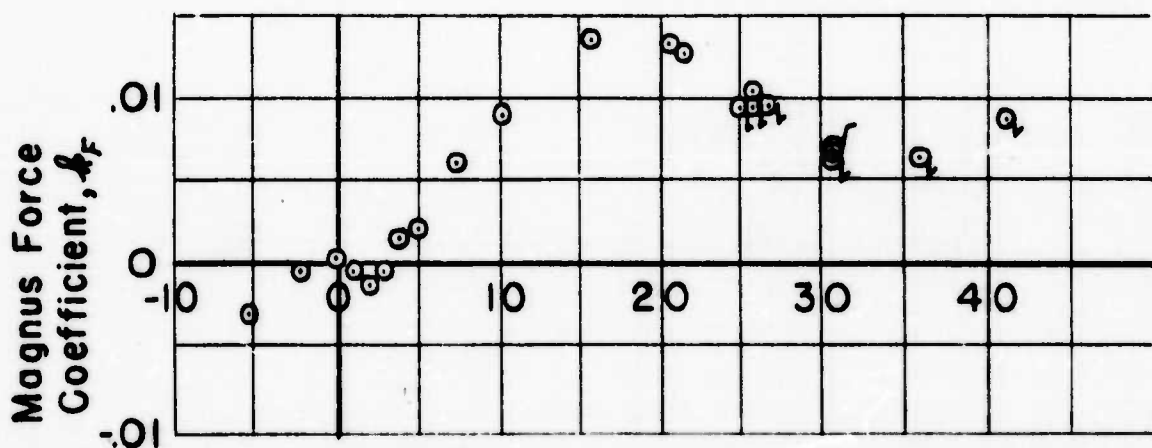
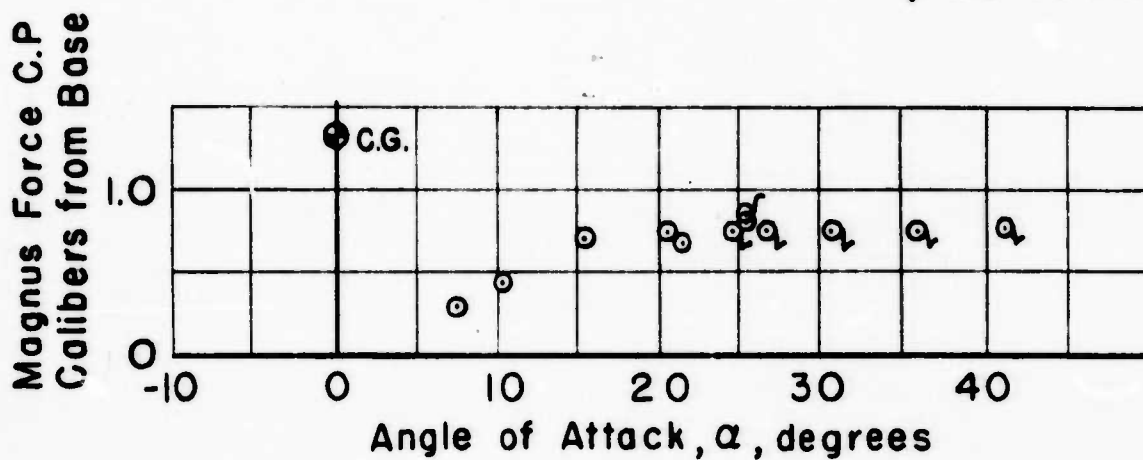
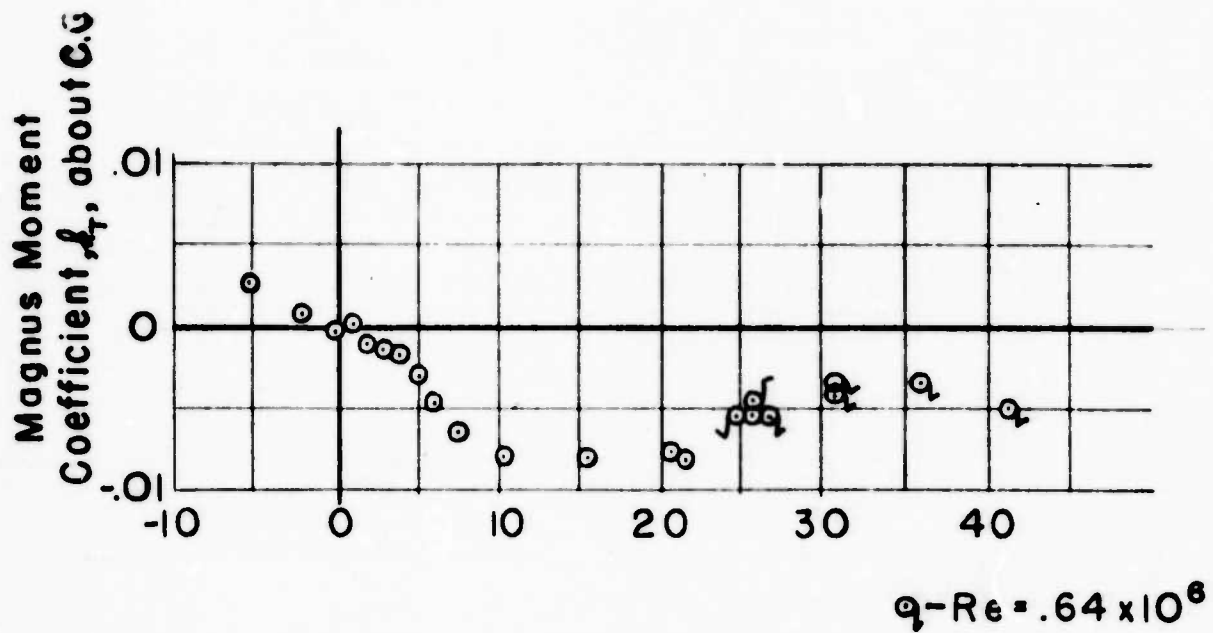
MAGNUS DATA FOR 30 MM BULLET

$Ma=1.57$

$\frac{\omega d}{u} = .536$

$Re = .75 \times 10^6$  Fig.25

CONFIDENTIAL



MAGNUS DATA FOR 30 MM BULLET

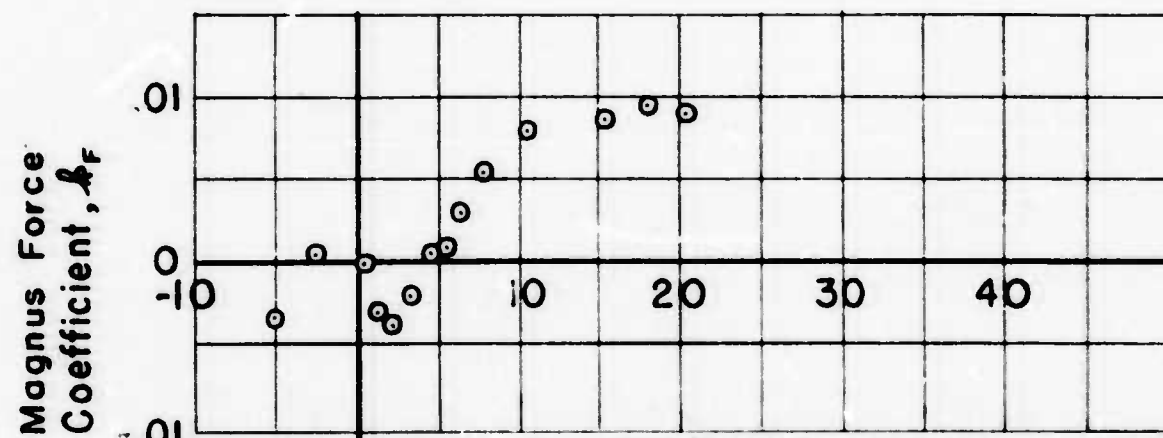
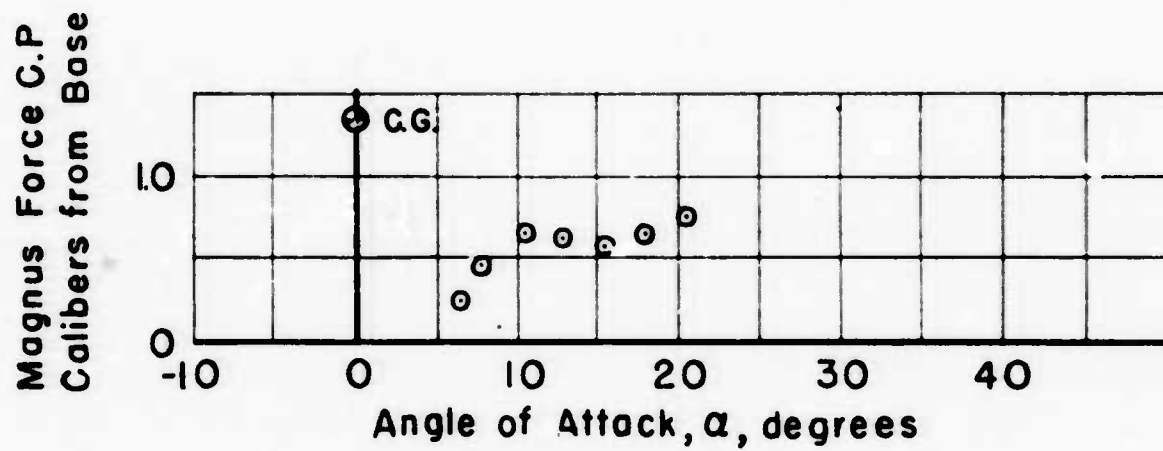
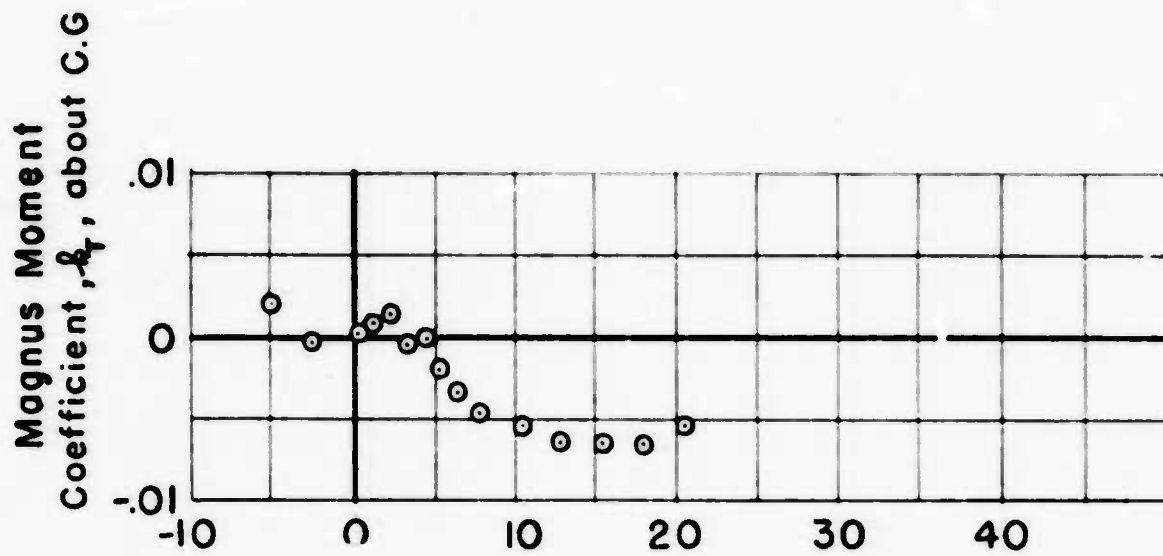
$Ma = 2.00$

$\frac{wd}{u} = 423$

$Re = .94 \times 10^6$

Fig.26

CONFIDENTIAL



MAGNUS DATA FOR 30 MM BULLET

$Ma = 2.47$

$\frac{\omega d}{U} = .335$

$Re = .76 \times 10^6$

Fig.27

CONFIDENTIAL

# CONFIDENTIAL

## APPENDIX I

### METHOD OF CALIBRATION AND DATA REDUCTION FOR A FOUR COMPONENT STRAIN GAGE BALANCE FOR MEASURING MAGNUS AND NORMAL FORCES

The aerodynamic forces and moments on the spinning model are measured using a four component strain gage balance shown in Fig. 26. The two pitch hinge lines and the two yaw hinge lines are approximately three inches apart and the front pitch and yaw hinge lines and the rear pitch and yaw hinge lines are roughly perpendicular to one another. The direction angles between the hinge lines and the normal, Magnus and axial drag directions are denoted in Fig. 26. The hinge lines are not parallel or perpendicular to one another nor in the planes of the normal, Magnus and drag forces due to unavoidable inaccuracies in centering the strain gages on the beam, to flow inclination, and misalignment of the balance in the tunnel. Hence for an accurate reduction of the data the following analysis must be made.

The moments about each hinge line produced by normal and Magnus forces can be written as

$$k_F m_F = N X_N \cos \beta_F + M.F. (X_N + C) \cos \gamma_F$$

$$k_R m_R = N (X_N + a) \cos \beta_R + M.F. (X_N + C + a) \cos \gamma_R$$

$$k_F m_F = N (X_N + C) \cos \eta_F + M.F. X_N \cos \epsilon_F$$

$$k_R m_R = N (X_N + C + b) \cos \eta_R + M.F. (X_N + b) \cos \epsilon_R$$

where

$k_F$ ,  $k_R$ ,  $k_F$ , and  $k_R$  are the front pitch, rear pitch, front yaw and rear yaw gage constants respectively.  $m_F$ ,  $m_R$ ,  $m_F$ ,  $m_R$  are the potentiometer moment readings about the front pitch, rear pitch, front yaw and rear yaw hinge lines respectively. The other symbols are defined in Fig. 26.

The distances a, b, and c; the direction angles; and the gage constants must be determined from calibration and test data before the normal and Magnus forces and their centers of pressure can be determined.

# CONFIDENTIAL

The moments about the hinge lines produced by hanging calibration weights at each of the six positions shown in Fig. 28, can be written in terms of the unknown parameters and the data recorded during the calibration (Table 1). This makes a total of 24 possible equations of which only 16 are required. Some equations will give identical results while others will give less accurate results due to small moments or the appearance of cosines of small angles. The 16 unknowns are  $K_F$ ,  $K_R$ ,  $K_F$ ,  $K_F$ ,  $X_N$ ,  $a$ ,  $b$ ,  $c$ ,  $\beta_F$ ,  $\beta_R$ ,  $\gamma_F$ ,  $\gamma_R$ ,  $\epsilon_F$ ,  $\epsilon_R$ ,  $\eta_F$  and  $\eta_R$ .

Before applying the calibration results to the wind tunnel data the calibration direction angles must be converted into the positions of the yaw and pitch hinge lines with respect to one another. This is necessary for the hinge line direction angles are dependent on the roll orientations of the balance. The relation between the hinge lines can be written as:

$$\cos \phi_F = \cos \beta_F \cos \eta_F + \cos \gamma_F \cos \epsilon_F + \cos \delta_F \cos \tau_F$$

$$\cos \phi_R = \cos \beta_R \cos \eta_R + \cos \gamma_R \cos \epsilon_R + \cos \delta_R \cos \tau_R$$

$$\cos \psi_Y = \cos \eta_F \cos \eta_R + \cos \epsilon_F \cos \epsilon_R + \cos \tau_F \cos \tau_R$$

where  $\phi_F$ ,  $\phi_R$ , and  $\psi_Y$  are essentially the angles between the front pitch and yaw hinge lines, the rear pitch and yaw hinge lines and the front and rear yaw lines respectively.

The direction angles for the test conditions are determined from the zero spin test data at each angle of attack. For zero spin the moment equations become:

$$K_F m_F = N X_N \cos \beta_F$$

$$K_R m_R = N(X_N + a) \cos \beta_R$$

$$K_F m_F = N(X_N + c) \cos \eta_F$$

$$K_F m_F = N(X_N + c + b) \cos \eta_R$$

Here  $\beta_F$ ,  $\beta_R$ ,  $\eta_F$ ,  $\eta_R$  are the test angles while previously the same symbols denote the corresponding calibration angles.

The hinge line relations  $\phi_F$ ,  $\phi_R$ , and  $\psi_Y$  can also be written in terms of the test hinge line direction angles so that ten equations are available to solve for ten unknowns (eight test hinge line direction angles plus the normal force and its center of pressure).

## CONFIDENTIAL

Once the test direction angles are known, the test data obtained while the model is spinning can be inserted in the main moment equations and the equations solved for the normal, and Magnus forces and their centers of pressure.

Simplifications to the above procedure can be made which will not impair the accuracy of the results. The simplifications are: 1) The direction angles  $\delta_T$ ,  $\delta_N$ ,  $\gamma_T$  and  $\gamma_N$  are the same for both calibration and test. This is because the model centerline or drag centerline is rigid with respect to the balance hinge lines. 2) The change in normal force with spin is negligible so that the normal force interaction with the yaw gages is constant except for strut deflections. 3) If the direction angles  $\epsilon_T$ ,  $\epsilon_N$ ,  $\beta_T$ , and  $\beta_N$  are small then their cosines may be taken equal to 1 and if the angles  $\gamma_T$ ,  $\gamma_N$ ,  $\eta_T$ , and  $\eta_N$  are close to  $90^\circ$ , their cosines may be assumed equal to 0. In order to determine if these assumptions are valid, it is necessary to compute, for a few critical cases, the Magnus force and its center of pressure with and without the above assumption.

# CONFIDENTIAL

TABLE I  
CALIBRATION EQUATIONS

For Vertical Force  $N_1$

- (1)  $k_F \frac{m_1^1}{m_2^1} = N_1 \cos \beta_F X_N$
- (2)  $k_F \frac{m_1^1}{m_2^1} = N_1 \cos \beta_F (X_N + a)$
- (3)  $k_F \frac{m_1^1}{m_2^1} = N_1 \cos \gamma_F (X_N + c)$
- (4)  $k_F \frac{m_1^1}{m_2^1} = N_1 \cos \gamma_F (X_N + c + b)$

For Vertical Force  $N_2$

- (5)  $k_F \frac{m_1^2}{m_2^2} = N_2 \cos \beta_F (X_N + d)$
- (6)  $k_F \frac{m_1^2}{m_2^2} = N_2 \cos \beta_F (X_N + a + d)$
- (7)  $k_F \frac{m_1^2}{m_2^2} = N_2 \cos \gamma_F (X_N + c + d)$
- (8)  $k_F \frac{m_1^2}{m_2^2} = N_2 \cos \gamma_F (X_N + c + b + d)$

For Horizontal Force M.F.<sub>3</sub>

- (9)  $k_F \frac{m_1^3}{m_2^3} = M.F._3 \cos \gamma_F (X_N)$
- (10)  $k_F \frac{m_1^3}{m_2^3} = M.F._3 \cos \gamma_F (X_N + a)$
- (11)  $k_F \frac{m_1^3}{m_2^3} = M.F._3 \cos \epsilon_F (X_N + c)$
- (12)  $k_F \frac{m_1^3}{m_2^3} = M.F._3 \cos \epsilon_F (X_N + c + b)$

For Horizontal Force M.F.<sub>4</sub>

- (13)  $k_F \frac{m_1^4}{m_2^4} = M.F._4 \cos \gamma_F (X_N + d)$
- (14)  $k_F \frac{m_1^4}{m_2^4} = M.F._4 \cos \gamma_F (X_N + a + d)$
- (15)  $k_F \frac{m_1^4}{m_2^4} = M.F._4 \cos \epsilon_F (X_N + c + d)$
- (16)  $k_F \frac{m_1^4}{m_2^4} = M.F._4 \cos \epsilon_F (X_N + c + b + d)$

# CONFIDENTIAL

For Vertical Force  $N_F$

$$(17) \quad X_F = \frac{\bar{S}}{\bar{F}} = N_F \left[ X_N \cos \theta_F + \bar{P} \cos \theta_F \right]$$

$$(18) \quad X_F = \frac{\bar{S}}{\bar{F}} = N_F \left[ (X_N + a) \cos \theta_F + \bar{P} \cos \theta_F \right]$$

$$(19) \quad X_F = \frac{\bar{S}}{\bar{F}} = N_F \left[ (X_N + c) \cos \theta_F + \bar{P} \cos \theta_F \right]$$

$$(20) \quad X_F = \frac{\bar{S}}{\bar{F}} = N_F \left[ (X_N + c + b) \cos \theta_F + \bar{P} \cos \theta_F \right]$$

For Horizontal Force  $M.F.C.$

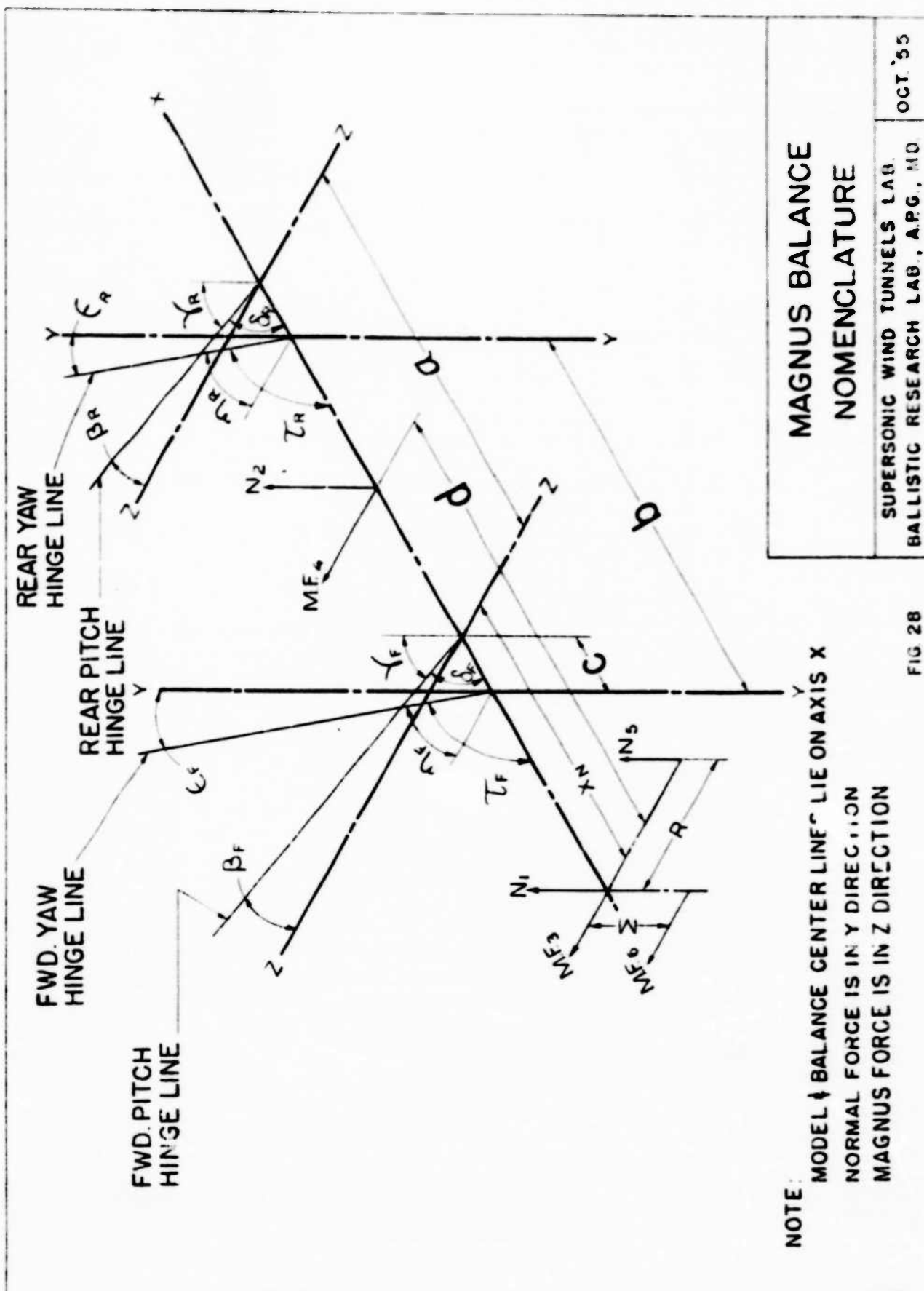
$$(21) \quad X_F = \frac{\bar{S}}{\bar{F}} = M.F.C. \left[ X_N \cos \gamma_F + M \cos \gamma_F \right]$$

$$(22) \quad X_F = \frac{\bar{S}}{\bar{F}} = M.F.C. \left[ (X_N + a) \cos \gamma_F + M \cos \gamma_F \right]$$

$$(23) \quad X_F = \frac{\bar{S}}{\bar{F}} = M.F.C. \left[ (X_N + c) \cos \gamma_F + M \cos \gamma_F \right]$$

$$(24) \quad X_F = \frac{\bar{S}}{\bar{F}} = M.F.C. \left[ (X_N + c + b) \cos \gamma_F + M \cos \gamma_F \right]$$





# DISTRIBUTION LIST

<u>No. of Copies</u>	<u>Organization</u>	<u>No. of Copies</u>	<u>Organization</u>
4	Chief of Ordnance Department of the Army Washington 25, D. C. Attn: ORDTB - Bal Sec ORDTX - AR ORDTS ORDTA	2	Commander Naval Air Missile Test Center Point Mugu, California
10	British Joint Ser. Mission 1600 K Street, N. W. Washington 6, D. C. Attn: Mr. John Inward, Reports Officer	1	Commanding Officer Naval Air Dev. Center Johnsville, Pa.
4	Canadian Army Staff 2450 Mass. Avenue Washington 6, D. C. Of Interest To: Dr. G.V. Bull CARDE	1	Commanding Officer and Director David W. Taylor Model Basin Washington 7, D. C. Attn: Aerodynamics Lab.
3	Chief, Bureau of Ordnance Department of the Navy Washington 25, D. C. Attn: ReO, J. D. Nicolsider	1	Commander Air University Maxwell Air Force Base, Alabama Attn: Air Univ. Library
1	Superintendent Naval Postgraduate School Monterey, California	1	Commander Arnold Eng. Dev. Center Tullahoma, Tennessee Attn: Deputy Chief of Staff, R&D
1	Commander Naval Proving Ground Dahlgren, Virginia	1	Commander Air Research and Dev. Command P. O. Box 1395 Baltimore 5, Md. Attn: RDTFAG
3	Commander Naval Ordnance Laboratory White Oak Silver Spring 19, Md. Of Interest to: Dr. H. K. H. K. Dr. E. Krahn Tech. Library	1	Commanding General Wright Air Dev. Center Wright-Patterson Air Force Base, Ohio Attn: Mr. E. Mott WOLSW-42
2	Commander Naval Ord. Test Station China Lake, California Attn: Tech. Library Dr. H. R. Kelly	4	Commander Air Force Armament Center Eglin Air Force Base, Florida Attn: ACR ASOTT ACE ACW ACRG

# DISTRIBUTION LIST

<u>No. of Copies</u>	<u>Organization</u>	<u>No. of Copies</u>	<u>Organization</u>
5	Director National Advisory Committee for Aeronautics 1512 H. Street, N. W. Washington 25, D. C. Attn: Div. Research Inf.	2	U. S. Atomic Energy Comm. Sandia Corporation P.O. Box 5400 Albuquerque, New Mexico Attn: Mrs. W. K. Cox
3	Director National Advisory Committee for Aeronautics Ames Laboratory Moffett Field, California Attn: Dr. A.C. Charters Mr. H.J. Allen Mr. A. Eggers	5	Director Armed Ser. Tech. Inf. Agency Documents Ser. Center Knott Building Dayton 2, Ohio Attn: DSC - SD
3	Director National Advisory Committee for Aeronautics Langley Memorial Aero. Lab. Langley Field, Virginia Attn: Mr. J. Bird Mr. C.E. Brown Dr. A. Busemann	1	Chief, Armed Forces Special Weapons Project P.O. Box 2610 Washington 25, D. C.
1	Director National Advisory Committee for Aeronautics Lewis Flight Propulsion Lab. Cleveland Airport Cleveland, Ohio Attn: EVAARD	3	Commanding General Redstone Arsenal Huntsville, Alabama
2	Director, JPL Ord. Corp. Installation Department of the Army 4800 Oak Grove Drive Pasadena 3, California Attn: Mr. Irl E. Newlan, Reports Group	3	Commanding General Picatinny Arsenal Dover, New Jersey Attn: Samuel Feltman Ammunition Labs.
1	Director National Bureau of Standards Conn. Ave. and Van Ness St. N.W. Attn: G. B. Schubauer	2	Commanding General Frankford Arsenal Philadelphia, Pa.
		1	Commanding Officer Chemical Corps Chemical and Radiological Lab. Army Chemical Center, Md.
		1	Director, Operations Research Office 7100 Conn. Avenue Chevy Chase, Md. Washington 15, D. C.

# DISTRIBUTION LIST

<u>No. of Copies</u>	<u>Organization</u>	<u>No. of Copies</u>	<u>Organization</u>
2	Armour Research Foundation Ill. Institute of Tech. Technology Center Chicago 16, Illinois Attn: Mr. W.W. Casler Dr. A. Wundheiler  TERU: District Chief Chicago Ord. Dist. 209 W. Jackson Blvd. Chicago 6, Illinois	1	Cornell University Graduate School of Aero. Ithica, New York  TERU: National Advisory Committee for Aeronautics 1512 K Street, N.W. Wash. 25, D. C.
1	A. B. Little, Inc. 30 Memorial Drive Cambridge 42, Massachusetts  TERU: Deputy Dist. Chief Boston Ord. Dist. Boston Army Base Boston 10, Mass.	2	Cornell Aero. Lab., Inc. Buffalo, New York Attn: Miss Elma T. Evans, Librarian Of Interest to: Mr. W.B. Young  TERU: Bureau of Aero. Representative Cornell Aero. Lab., Inc. P.O. Box 233 Buffalo 21, New York
1	Aerophysics Dev. Corporation P.O. Box 657 Pacific Palisades, California Attn: Dr. William Bolloy  TERU: District Chief Los Angeles Ord. Dist. 55 S. Grand Avenue Pasadena 2, California	1	CONVAIR Div. of General Dynamics Corp. Ord. Aerophysics Lab. Daingerfield, Texas Attn: Mr. J.E. Arnold  TERU: Asst. Inspector of Naval Material Ord. Aerophysics Lab. Daingerfield, Texas
1	ARO, Inc. Tullahoma, Tennessee Attn: Mr. R. Smelt  TERU: Deputy Dist. Chief Cincinnati Ord. Dist. Big Four Building Cincinnati 2, Ohio	1	Firestone Tire and Rubber Company Defense Research Div. Akron 17, Ohio Attn: Peter J. Ginge  TERU: Deputy Dist. Chief Cleveland Ord. Dist. Lincoln Bldg. 1367 E. 6th St. Cleveland 14, Ohio
2	Applied Physics Laboratory 8621 Georgia Avenue Silver Spring, Maryland  TERU: Naval Inspector of Ord. Applied Physics Lab. Johns Hopkins University 8621 Georgia Avenue Silver Spring, Md.		

# DISTRIBUTION LIST

<u>No. of Copies</u>	<u>Organization</u>	<u>No. of Copies</u>	<u>Organization</u>
1	Guggenheim Aero. Lab. California Inst. of Tech. Pasadena 4, Calif. Attn: Professor H.W. Liepman  THRU: District Chief Los Angeles Ord. Dist. 55 S. Grand Avenue Pasadena 2, Calif.	1	North Carolina State College Raleigh, North Carolina Attn: Prof. J. W. Cell  THRU: Deputy Dist. Chief Philadelphia Ord. Dist. 128 North Broad St. Philadelphia 2, Pa.
1	General Electric Company Library, GM Department 2900 Campbell Avenue Schenectady 6, New York Attn: Jack M. McCormick  THRU: Air Force Plant Rep. General Electric Co. 1 River Road Schenectady, New York	1	Princeton University Aero. Department Princeton, New Jersey Attn: Prof. Wallace Hayes  THRU: National Advisory Committee for Aeronautics 1512 E Street, N.W. Wash. 25, D. C.
1	M. W. Kellogg Company Foot of Danforth Avenue Jersey City 3, New Jersey Attn: Miss E.M. Hedley  THRU: Inspector of Naval Material Naval Industrial Reserve Shipyard Building 24, Port Newark Newark 5, New Jersey	2	United Aircraft Corp. Research Dept. East Hartford 8, Conn. Attn: Mr. Robert C. Sale Mr. M. Schweiger  THRU: Bureau of Aero. Representative Pratt and Whitney Aircraft Div. United Aircraft Corp. East Hartford 8, Conn.
2	Mass. Institute of Technology Instrumentation Lab. 155 Mass. Avenue Cambridge 39, Mass. Attn: Dr. C.S. Draper  THRU: Inspector of Naval Material Mass. Institute of Tech. Cambridge 39, Mass. Attn: Dev. Contract Dept.	1	Univ. of Southern Calif. Engineering Center Los Angeles 7, Calif. Attn: Mr. H.R. Saffell, Director  THRU: Bureau of Aero. Rep. Aerojet Eng. Corp. 6352 N. Irwindale Ave. Azusa, Calif.

# DISTRIBUTION LIST

<u>No. of Copies</u>	<u>Organization</u>	<u>No. of Copies</u>	<u>Organization</u>
1	University of Michigan Willow Run Research Center Willow Run Airport Ypsilanti, Michigan Attn: Mr. J.E. Corey	1	Professor E.W. Emmons Harvard University Cambridge 38, Mass.
	TERU: Commander Central Air Procurement District West Warren and Long Avenues Detroit 32, Michigan.	1	Dr. Clark E. Millikan Calif. Instit. of Tech. Pasadena, Calif.
1	Wright Aero. Corporation Wood-Ridge, New Jersey Attn: Sales Dept (Government)	1	Dr. A.E. Puckett Hughes Aircraft Co. Florence Ave. at Teul St. Culver City, Calif.
	TERU: Air Force Plant Rep. Wright Aero. Corporation Wood-Ridge, New Jersey	1	Dr. L.H. Thomas Watson Scientific Computing Lab. 612 West 116th Street New York 27, New York
1	Professor George Carrier Div. of Applied Sciences Harvard University Cambridge 38, Mass.	1	Naval Supersonic Lab. Mass. Institute of Tech. Cambridge 39, Mass. Attn: Mr. Frank E. Dargis
		1	Office, Assistant Secretary of Defense (R&D) Committee on Ordnance Washington 25, D. C.